AD-A133 203 RADIATION PATTERNS OF AN ANTENNA MOUNTED ON THE MID-SECTION OF AN ELLIPSOID(U) OHIO STATE UNIV COLUMBUS ELECTROSCIENCE LAB J G KIM ET AL. JUL 83 ESL-714215-2 1/1

UNCLASSIFIED N00019-81-C-0424 F/G 20/14 NL

END
DATE
FILMED
10 83
DTIC

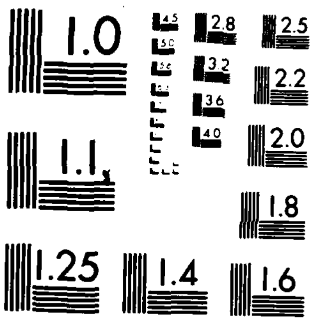

MICROCOPY RESOLUTION TEST CHART
NATIONAL BUREAU OF STANDARDS 1963-A

(12)

AD-A133203

The Ohio State University

RADIATION PATTERNS OF AN ANTENNA MOUNTED ON THE

MID-SECTION OF AN ELLIPSOID

Jeung G. Kim
Walter D. Burnside

The Ohio State University

ElectroScience Laboratory

Department of Electrical Engineering
Columbus, Ohio 43212

Quarterly Report 714215-2

Contract No. N00019-81-C-0424

July 1983

Department of the Navy
Naval Air Systems Command
Washington, D.C. 20361

NOTICES

When Government drawings, specifications, or other data are used for any purpose other than in connection with a definitely related Government procurement operation, the United States Government thereby incurs no responsibility nor any obligation whatsoever, and the fact that the Government may have formulated, furnished, or in any way supplied the said drawings, specifications, or other data, is not to be regarded by implication or otherwise as in any manner licensing the holder or any other person or corporation, or conveying any rights or permission to manufacture, use, or sell any patented invention that may in any way be related thereto.

50272-101

REPORT DOCUMENTATION PAGE	1. REPORT NO.	2. AD-A133203	3. Recipient's Accession No

4. Title and Subtitle

RADIATION PATTERNS OF AN ANTENNA MOUNTED ON THE MID-SECTION OF AN ELLIPSOID

5. Report Date

July 1983

6.

7. Author(s)

Jeung G. Kim and Walter D. Burnside

8. Performing Organization Rept. No

ESL-714215-2

9. Performing Organization Name and Address

The Ohio State University ElectroScience Laboratory
Department of Electrical Engineering
Columbus, Ohio 43212

10. Project/Task/Work Unit No.

11. Contract(C) or Grant(G) No

(C)

(G) N00019-81-C-0424

12. Sponsoring Organization Name and Address

Department of the Navy
Naval Air Systems Command
Washington, D.C. 20361

13. Type of Report & Period Covered

Quarterly Report

14.

15. Supplementary Notes

16. Abstract (Limit: 200 words)

An efficient numerical solution for the high frequency radiation patterns of an Antenna mounted on the Mid-Section ($\theta_s = 90°$) of an Ellipsoid is studied in this report. The Uniform Geometrical Theory of Diffraction (UTD) [1,3] is the basic approach applied here and the elliptic cylinder perturbation method [1,2] is used to simulate geodesic paths on the ellipsoid surface. The radiation patterns obtained using this technique are compared to those for prolate spheriod-mounted antennas, which have shown good agreement with measured data. Exact agreement between both results for typical spheroid geometry confirms that radiation patterns for ellipsoid mounted antennas can be solved efficiently by this numerical technique.

17. Document Analysis a. Descriptors

b. Identifiers/Open-Ended Terms

c. COSATI Field/Group

18. Availability Statement	19. Security Class (This Report)	21. No of Pages
APPROVED FOR PUBLIC RELEASE; DISTRIBUTION UNLIMITED	Unclassified	43
	20. Security Class (This Page) Unclassified	22. Price

(See ANSI-Z39.18) See Instructions on Reverse OPTIONAL FORM 272 (4-77) (Formerly NTIS-35) Department of Commerce

TABLE OF CONTENTS

LIST OF FIGURES

Figure		Page

I. INTRODUCTION

In applying the Uniform Geometrical Theory of Diffraction (UTD) to antenna radiation problem involving curved surfaces, a major task is to determine the final diffraction point and the geodesic path on that surface. For the antennas mounted on the fuselage of an aircraft, the fuselage can be modeled as an ellipsoid in the UTD analysis. Geodesic paths on an ellipsoid have been studied in detail in References [1,2] using an elliptic cylinder perturbation method which is very efficient.

Using this perturbation method and another numerical technique, which will be given in this report, the radiation patterns for ellipsoid mounted antennas is efficiently obtained. The theoretical UTD concept employed to calculate the actual radiation fields is given in Reference [1,3].

II. NUMERICAL TECHNIQUE

A. INTRODUCTION

The ellipsoid simulated by a perturbed elliptic cylinder model is examined here. Since the elliptic cylinder is a developable surface, geodesics can be easily obtained [1,2]. Given a radiation direction (θ_t, ϕ_t), one can find the final diffraction point (θ_Q, ϕ_Q) by following the geodesic path, step by step, until the geodesic tangent coincides

with the radiation direction (θ_t, ϕ_t). This is a rather tedius and time consuming process if applied for each new radiation direction. Considering a new radiation direction, which does not deviate greatly from the previous direction, one should be able to develop a solution which uses the properties of the surface and the previous geodesic path to find the new diffraction point. Such an approach is attempted here to make this solution as efficient as possible.

Since the field decays exponentially along the ray path on the surface, it is assumed that only one or possibly two dominant rays exist in the problems treated. One is referred to References [1,2] for more details on this topic.

B. NUMERICAL APPROACH FOR PATTERN CALCULATION

Assuming the diffraction point is located at Q ($a \cos v_e \cos v_r$, $b \cos v_e \sin v_r$, $c \sin v_e$) and the field point at P ($R_t \sin \theta_t \cos \phi_t$, $R_t \sin \theta_t \sin \phi_t$, $R_t \cos \theta_t$), then at the diffraction point Q the radiation direction (θ_t, ϕ_t) should coincide with the geodesic tangent $\hat{t}$ as shown in Figure 1. Thus,

$$\hat{t} = \hat{x}\, t_x + \hat{y}\, t_y + \hat{z}\, t_z$$

$$= \hat{t}_1 \cos \gamma + \hat{t}_e \sin \gamma \quad ,$$

where

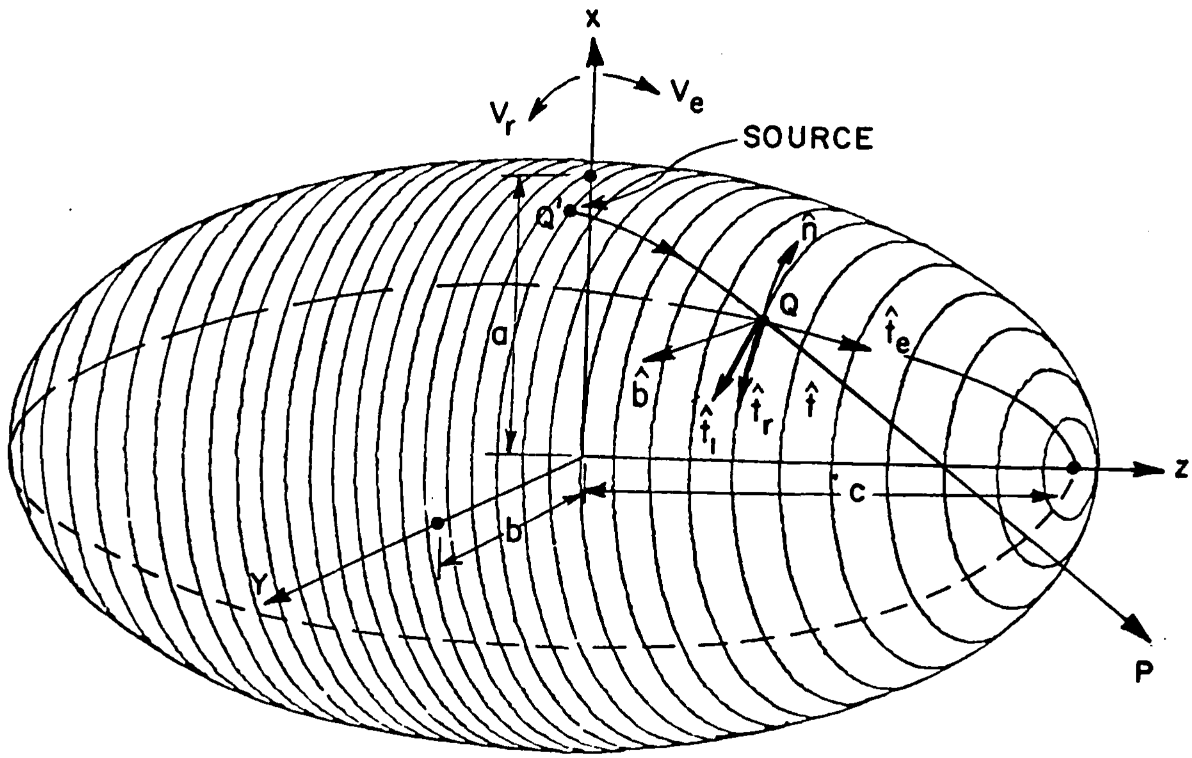

Figure 1. Geodesic path from the source on an ellipsoid.

$$t_x = \frac{\sin\theta_t \cos\phi_t - \frac{a}{R_t}\cos v_e \cos v_r}{D}$$

$$t_y = \frac{\sin\theta_t \sin\phi_t - \frac{b}{R_t}\cos v_e \cos v_r}{D}$$

and

$$t_z = \frac{\cos\theta_t - \frac{c}{R_t}\sin v_e}{D} \quad .$$

Note that

$$D^2 = (\sin\theta_t \cos\phi_t - \frac{a}{R_t}\cos v_e \cos v_r)^2 + (\sin\theta_t \sin\phi_t$$

$$- \frac{b}{R_t}\cos v_e \sin v_r)^2 + (\cos\theta_t - \frac{c}{R_t}\sin v_e)^2$$

$$= 1 - 2[\sin\theta_t \cos v_e \; (\frac{a}{R_t}\cos\phi_t \cos v_r + \frac{b}{R_t}\sin\phi_t \sin v_r)$$

$$+ \frac{c}{R_t}\cos\theta_t \sin v_e] + [\cos^2 v_e \; (\frac{a^2}{R_t^2}\cos^2 v_r + \frac{b^2}{R_t^2}\sin^2 v_r) + \frac{c^2}{R_t^2}\sin^2 v_e]$$

, and

$$\hat{t}_1 = \hat{t}_e \times \hat{n}$$

$$= \frac{-\hat{x} a \sin v_r (b^2 \sin^2 v_e + c^2 \cos^2 v_e) + \hat{y} b \cos v_r (a^2 \sin^2 v_e + c^2 \cos^2 v_e)}{[a^2 b^2 \sin^2 v_e + c^2 \cos^2 v_e (a^2 \sin^2 v_r + b^2 \cos^2 v_r)]^{1/2}} - -$$

$$- - - - \frac{+\hat{z} c (b^2 - a^2) \sin v_r \cos v_r \sin v_e \cos v_e}{[c^2 \cos^2 v_e + \sin^2 v_e (a^2 \cos^2 v_r + b^2 \sin^2 v_r)]^{1/2}}$$

where

$$\hat{t}_e = \frac{\dfrac{\partial \vec{R}}{\partial v_e}}{\left|\dfrac{\partial \vec{R}}{\partial v_e}\right|} = \frac{-\hat{x}a \sin v_e \cos v_r - \hat{y}b \sin v_e \sin v_r + \hat{z}c \cos v_e}{[a^2\sin^2 v_e \cos^2 v_r + b^2 \sin^2 v_e \sin^2 v_r + c^2 \cos^2 v_e]^{1/2}}$$

$$\hat{t}_r = \frac{\dfrac{\partial \vec{R}}{\partial v_r}}{\left|\dfrac{\partial \vec{R}}{\partial v_r}\right|} = \frac{-\hat{x}a \cos v_e \sin v_r + \hat{y}b \cos v_e \cos v_r}{[a^2\cos^2 v_e \sin^2 v_r + b^2 \cos^2 v_e \cos^2 v_r]^{1/2}}$$

and

$$\hat{n} = \frac{\hat{t}_r \times \hat{t}_e}{|\hat{t}_r \times \hat{t}_e|}$$

$$= \frac{\hat{x}bc \cos v_e \cos v_r + \hat{y}ac \cos v_e \sin v_r + \hat{z}ab \sin v_e}{[a^2b^2\sin^2 v_e + c^2\cos^2 v_e(a^2\sin^2 v_r + b^2\cos^2 v_r)]^{1/2}} .$$

Equating the x-, y-, and z- components, respectively, one obtains

$$t_x = \frac{-a \sin v_r \cos\gamma(b^2\sin^2 v_e + c^2\cos^2 v_e)}{[a^2b^2\sin^2 v_e + c^2\cos^2 v_e(a^2\sin^2 v_r + b^2\cos^2 v_r)]^{1/2}} \cdot$$

$$\cdot\ [c^2\cos^2 v_e + \sin^2 v_e(a^2\cos^2 v_r + b^2\sin^2 v_r)]^{1/2}$$

$$- \frac{a \sin v_e \cos v_r \sin\gamma}{[c^2\cos^2 v_e + \sin^2 v_e(a^2\cos^2 v_r + b^2\sin^2 v_r)]^{1/2}}$$

$$= \frac{\sin\theta_t \cos\phi_t - \frac{a}{R_t} \cos v_e \cos v_r}{D} \qquad (1)$$

$$t_y = \frac{b\cos v_r \cos\gamma(a^2\sin^2 v_e + c^2\cos v_e)}{[a^2b^2\sin^2 v_e + c^2\cos^2 v_e(a^2\sin^2 v_r + b^2\cos^2 v_r)]^{1/2} \cdot}$$

$$\cdot\ [c^2\cos^2 v_e + \sin^2 v_e(a^2\cos^2 v_r + b^2\sin^2 v_r)]^{1/2}$$

$$- \frac{b\sin v_e \sin v_r \sin\gamma}{[c^2\cos^2 v_e + \sin^2 v_e(a^2\cos^2 v_r + b^2\sin^2 v_r)]^{1/2}}$$

$$= \frac{\sin\theta_t \sin\phi_t - \frac{b}{R_t}\cos v_e \sin v_r}{D} \quad . \tag{2}$$

$$t_z = \frac{c(b^2-a^2)\sin v_r \cos v_r \sin v_e \cos v_e \cos\gamma}{[a^2b^2\sin^2 v_e + c^2\cos^2 v_e(a^2\sin^2 v_r + b^2\cos^2 v_r)]^{1/2} \cdot}$$

$$\cdot\ [c^2\cos^2 v_e + \sin^2 v_e(a^2\cos^2 v_r + b^2\sin^2 v_r)]^{1/2}$$

$$+ \frac{c\cos v_e \sin\gamma}{[c^2\cos^2 v_e + \sin^2 v_e(a^2\cos^2 v_r + b^2\sin^2 v_r)]^{1/2}}$$

$$= \frac{\cos\theta_t - \frac{c}{R_t}\sin v_e}{D} \quad . \tag{3}$$

When the source is located at the mid-section ($z = 0$ in Figure 1), the ellipsoid is modeled by a perturbed elliptic cylinder. The associated unfolded surface is shown in Figure 2(b). It is noticed that γ is a constant along the geodesic path as shown in the figure.

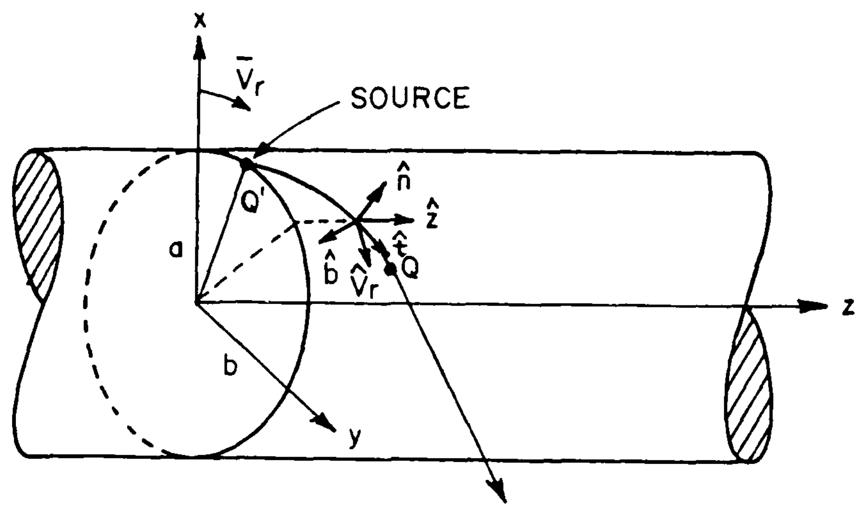

(a) TRUE ELLIPTIC CYLINDER

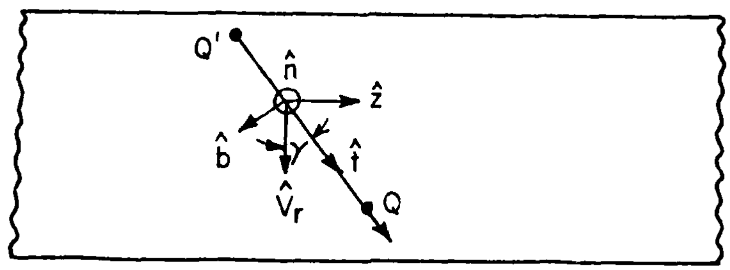

(b) UNFOLDED PLANAR SURFACE

Figure 2. Geodesic path on a developed elliptic cylinder.

Now, $[t_x b\cos V_r + t_y a\sin V_r] c\cos V_e + t_z ab\sin V_e$ yields

$$H(\theta_t, \phi_t, V_e, V_r, R_t)$$

$$= ab\sin V_e \cos\theta_t + c\sin\theta_t \cos V_e (a\sin\phi_t \sin V_r + b\cos\phi_t \cos V_r)$$

$$- \frac{abc}{R_t} = 0 \quad . \tag{4}$$

Next, from Equations (1) and (2) one obtains

$$t_x (-b \sin V_r) + t_y (a \cos V_r):$$

$$\frac{ab \cos\gamma\{\sin^2 V_e (b^2\sin^2 V_r + a^2\cos^2 V_r) + c^2\cos^2 V_e\}^{1/2}}{\{a^2b^2\sin^2 V_e + c^2\cos^2 V_e (a^2\sin^2 V_r + b^2\cos^2 V_r)\}^{1/2}}$$

$$= \frac{1}{D} \{a\cos V_r \sin\theta_t \sin\phi_t - b\sin V_r \sin\theta_t \cos\phi_t\} \quad .$$

Accordingly,

$$\cos\gamma = [a^2b^2\sin^2 V_e + c^2\cos^2 V_e(a^2\sin^2 V_r + b^2\cos^2 V_r)]^{1/2} \cdot$$

$$\cdot \frac{\sin\theta_t(a\cos V_r \sin\phi_t - b\sin V_r \cos\phi_t)}{Dab\{\sin^2 V_e(b^2\sin^2 V_r + a^2\cos^2 V_r) + c^2\cos^2 V_e\}^{1/2}} \quad . \tag{5}$$

Substituting Equation (5) into Equation (3),

$$\cdot\ (a\cos V_r \sin\phi_t - b\sin V_r \cos\phi_t)$$

$$\Big[c(b^2-a^2)\sin V_r \cos V_r \sin V_e \cos V_e \sin\theta_t\ \cdot$$

$$+\ c\cos V_e \frac{S_e}{S_r} \sin\theta_t\ (a\cos V_r \sin\phi_t - b\sin V_r \cos\phi_t)\ \cdot$$

$$\cdot\ \frac{\{a^2b^2\sin^2 V_e + c^2\cos^2 V_e(a^2\sin^2 V_r + b^2\cos^2 V_r)\}^{1/2}\ \Big]}{ab[c^2\cos^2 V_e + \sin^2 V_e(a^2\cos^2 V_r + b^2\sin^2 V_r)]}$$

$$= \cos\theta_t - \frac{c}{R_t}\sin V_e \quad .$$

Thus, one finds that

$$
\begin{aligned}
&G(\theta_t, \phi_t, V_e, V_r, R_t) \\
&\quad = S_r\, c(b^2-a^2)\sin V_r \cos V_r \sin V_e \cos V_e \sin\theta_t\ \cdot \\
&\quad \cdot\ (a\cos V_r \sin\phi_t - b\sin V_r \cos\phi_t) \\
&\quad + S_e\, c\cos V_e\ [a^2b^2\sin^2 V_e + c^2\cos^2 V_e(a^2\sin^2 V_r + b^2\cos^2 V_r)]^{1/2} \\
&\quad \cdot\ \sin\theta_t\ (a\cos V_r \sin\phi_t - b\sin V_r \cos\phi_t) \\
&\quad - S_r\, ab\cos\theta_t\ [c^2\cos^2 V_e + \sin^2 V_e(a^2\cos^2 V_r + b^2\sin^2 V_r)] \\
&\quad + \frac{S_r}{R_t} abc\sin V_e\ [c^2\cos^2 V_e + \sin^2 V_e(a^2\cos^2 V_r + b^2\sin^2 V_r)] \\
&\quad = 0 \quad . \qquad\qquad (6)
\end{aligned}
$$

where

$$S_e = \int_0^{V_e} \{c^2\cos^2V_e' + (a^2\cos^2V_r + b^2\sin^2V_r)\sin^2V_e'\}^{1/2} dV_e' \quad ,$$

and

$$S_r = \int_{V_{r_s}}^{V_r} \cos V_{es} \; \{a^2\sin^2V_r' + b^2\cos^2V_r'\}^{1/2} dV_r' \quad .$$

Provided that one has obtained a diffraction point (V_e, V_r) for a receiver location (R_t, θ_t, ϕ_t), a numerical technique can now be developed from Equations (4) and (6) to solve for ($V_e + \Delta V_e$, $V_r + \Delta V_r$) associated with a new receiver location ($R_t + \Delta R_t$, $\theta_t + \Delta\theta_t$, $\phi_t + \Delta\phi_t$). Assuming that the i^{th} set of (R_t, θ_t, ϕ_t, V_e, V_r) is first known to satisfy $H_i = G_i = 0$, or at least approximately so, the next set ($R_t + \Delta R_t$, $\theta_t + \Delta\theta_t$, $\phi_t + \Delta\phi_t$, $V_e + \Delta V_e$, $V_r + \Delta V_r$) is obtained by enforcing $H_{i+1} = G_{i+1} = 0$, such that

$$\begin{aligned} H_{i+1} &= H_i + H_{R_t}\Delta R_t + H_{\theta_t}\Delta\theta_t + H_{\phi_t}\Delta\phi_t + \\ &\quad H_{V_e}\Delta V_e + H_{V_r}\Delta V_r \\ &= 0 \end{aligned}$$

and

$$\begin{aligned} G_{i+1} &= G_i + G_{R_t}\Delta R_t + G_{\theta_t}\Delta\theta_t + G_{\phi_t}\Delta\phi_t + \\ &\quad + G_{V_e}\Delta V_e + G_{V_r}\Delta V_r \\ &= 0 \quad . \end{aligned}$$

In matrix form, it is given by

$$\begin{bmatrix} H_{V_e} & H_{V_r} \\ G_{V_e} & G_{V_r} \end{bmatrix} \begin{bmatrix} \Delta V_e \\ \Delta V_r \end{bmatrix} = \begin{bmatrix} -H_i - H_{R_t}\Delta R_t - H_{\theta_t}\Delta\theta_t - H_{\phi_t}\Delta\phi_t \\ -G_i - G_{R_t}\Delta R_t - G_{\theta_t}\Delta\theta_t - G_{\phi_t}\Delta\phi_t \end{bmatrix} . \qquad (7)$$

Note that the partial derivatives are given by the following:

$$H_{V_e} = ab \cos V_e \cos\theta_t - c \sin V_e \sin\theta_t (a \sin\phi_t \sin V_r + b\cos\phi_t \cos V_r)$$

$$H_{V_r} = c \cos V_e \sin\theta_t \ (a\sin\phi_t \cos V_r - b\cos\phi_t \sin V_r)$$

$$H_{\theta_t} = -ab \sin V_e \sin\theta_t + c \cos V_e \cos\theta_t (a\sin\phi_t \sin V_r + b\cos\phi_t \cos V_r)$$

$$H_{\phi_t} = c \cos V_e \sin\theta_t \ (a \cos\phi_t \sin V_r - b \sin\phi_t \cos V_r)$$

$$H_{R_t} = abc/R_t^2$$

$$G_{V_e} = S_r \ c(b^2-a^2) \sin V_r \cos V_r (\cos^2 V_e - \sin^2 V_e) \cdot$$

$$\cdot \sin\theta_t (a \cos V_r \sin\phi_t - b \sin V_r \cos\phi_t) +$$

$$+ \frac{dS_e}{dV_e} c \cos V_e [a^2b^2\sin^2 V_e + c^2\cos^2 V_e (a^2\sin^2 V_r + b^2\cos^2 V_r]^{1/2}$$

$$\cdot \sin\theta_t (a \cos V_r \sin\phi_t - b \sin V_r \cos\phi_t) +$$

$$+ S_e\, c \sin\theta_t (a \cos V_r \sin\phi_t - b \sin V_r \cos\phi_t) \sin V_e \;\cdot$$

$$\cdot \frac{a^2 b^2 (\cos^2 V_e - \sin^2 V_e) - 2c^2 \cos^2 V_e (a^2 \sin^2 V_r + b^2 \cos^2 V_r)}{[a^2 b^2 \sin^2 V_e + c^2 \cos^2 V_e (a^2 \sin^2 V_r + b^2 \cos^2 V_r)]^{1/2}}$$

$$+ 2\, S_r\, abc\cos\theta_t \cos V_e \sin V_e\, (c^2 - a^2 \cos^2 V_r - b^2 \sin^2 V_r)$$

$$+ \frac{S_r}{R_t}\, abc \cos V_e [c^2 \cos^2 V_e + \sin^2 V_e (a^2 \cos^2 V_r + b^2 \sin^2 V_r)$$

$$+ 2 \sin^2 V_e (a^2 \cos^2 V_r + b^2 \sin^2 V_r - c^2)]$$

where

$$\frac{dS_e}{dV_e} = \{c^2 \cos^2 V_e + (a^2 \cos^2 V_r + b^2 \sin^2 V_r) \sin^2 V_e\}^{1/2} \quad ,$$

$$G_{V_r} = \{ \frac{dS_r}{dV_r} \sin V_r \cos V_r + S_r (\cos^2 V_r - \sin^2 V_r)\} \;\cdot$$

$$\cdot\, c(b^2 - a^2) \sin V_e \cos V_e \sin\theta_t\, (a \cos V_r \sin\phi_t - b \sin V_r \cos\phi_t)$$

$$- S_r\, c(b^2 - a^2) \sin V_r \cos V_r \sin V_e \cos V_e \sin\theta_t \;\cdot$$

$$\cdot\, (a \sin V_r \sin\phi_t + b \cos V_r \cos\phi_t) \;+$$

$$+ \frac{dS_e}{dV_r}\, c \cos V_e [a^2 b^2 \sin^2 V_e + c^2 \cos^2 V_e (a^2 \sin^2 V_r + b^2 \cos^2 V_r)]^{1/2} \;\cdot$$

$$\cdot\, \sin\theta_t (a \cos V_r \sin\phi_t - b \sin V_r \cos\phi_t) \;+$$

$$+ \frac{S_e c^3 \cos^3 V_e (a^2 - b^2) \sin V_r \cos V_r \sin\theta_t (a\cos V_r \sin\phi_t - b\sin V_r \cos\phi_t)}{[a^2 b^2 \sin^2 V_e + c^2 \cos^2 V_e (a^2 \sin^2 V_r + b^2 \cos^2 V_r)]^{1/2}}$$

$$- S_e\, c \cos V_e [a^2 b^2 \sin^2 V_e + c^2 \cos^2 V_e (a^2 \sin^2 V_r + b^2 \cos^2 V_r)]^{1/2} \cdot$$

$$\cdot \sin\theta_t (a \sin V_r \sin\phi_t + b \cos V_r \cos\phi_t)$$

$$- \frac{dS_r}{dV_r} ab \cos\theta_t [c^2 \cos^2 V_e + \sin^2 V_e (a^2 \cos^2 V_r + b^2 \sin^2 V_r)]$$

$$+ 2S_r\, ab(a^2 - b^2) \cos\theta_t \sin^2 V_e \cos V_r \sin V_r$$

$$+ \frac{dS_r}{dV_r} \frac{abc}{R_t} \sin V_e [c^2 \cos^2 V_e + \sin^2 V_e (a^2 \cos^2 V_r + b^2 \sin^2 V_r)]$$

$$+ \frac{2S_r}{R_t} abc \sin^3 V_e (b^2 - a^2) \cos V_r \sin V_r$$

where

$$\frac{dS_r}{dV_r} = \cos V_{es} \{a^2 \sin^2 V_r + b^2 \cos^2 V_r\}^{1/2} \quad ,$$

and

$$\frac{dS_e}{dV_r} = \int_0^{V_e} \frac{(b^2 - a^2) \sin V_r \cos V_r \sin^2 V_e'}{[c^2 \cos^2 V_e' + (a^2 \cos^2 V_r + b^2 \sin^2 V_r) \sin^2 V_e']^{1/2}} dV_e' \quad .$$

$$G_{\theta_t} = S_r\, c(b^2 - a^2) \sin V_r \cos V_r \sin V_e \cos V_e \cos\theta_t \quad \cdot$$

$$\cdot (a \cos V_r \sin\phi_t - b \sin V_r \cos\phi_t) +$$

$$+ S_e\, c \cos V_e [a^2 b^2 \sin^2 V_e + c^2 \cos^2 V_e (a^2 \sin^2 V_r + b^2 \cos^2 V_r)]^{1/2} \quad \cdot$$

$$\cdot \cos\theta_t(a \cos V_r \sin\phi_t - b \sin V_r \cos\phi_t) +$$

$$+ S_r\, ab \sin\theta_t [c^2\cos^2 V_e + \sin^2 V_e(a^2\cos^2 V_r + b^2\sin^2 V_r)]$$

$$G_{\phi_t} = S_r\, c(b^2-a^2) \sin V_r \cos V_r \sin V_e \cos V_e \sin\theta_t \quad \cdot$$

$$\cdot\ (a \cos V_r \cos\phi_t - b \sin V_r \sin\phi_t) +$$

$$+ S_e\, c \cos V_e [a^2b^2\sin^2 V_e + c^2\cos^2 V_e(a^2\sin^2 V_r + b^2\cos^2 V_r)]^{1/2} \quad \cdot$$

$$\cdot \sin\theta_t(a \cos V_r \cos\phi_t + b \sin V_r \sin\phi_t)$$

$$G_{R_t} = -\frac{S_r}{R_t^{\,2}}\, abc \sin V_e [c^2\cos^2 V_e + \sin^2 V_e(a^2\cos^2 V_r + b^2\sin^2 V_r)] \quad .$$

It is seen that one can solve for $(\Delta V_e, \Delta V_r)$, for a known $(\Delta R_t, \Delta\theta_t, \Delta\phi_t)$, using Equation (7). To determine the initial diffraction point (V_e, V_r) for a given receiver location (R_t, θ_t, ϕ_t), one can always assume a diffraction point at the source $(0, V_{r_s})$ with the radiation direction $(\theta_f, \phi_f = \pm \frac{\pi}{2})$ with respect to the source coordinate system $(\hat{t}_N, \hat{t}_r, \hat{t}_e)$ and gradually add increments $(\Delta R_t, \Delta\theta_t, \Delta\phi_t)$ until the desired receiver location (R_t, θ_t, ϕ_t) is reached as depicted in Figure 3.

In this process one can construct a cone where the rim of the cone is traced out by the receiver trajectery with the tip of the cone at the source point Q' and the cone axis aligned with $\hat{t}_e$. The half cone angle θ_f is given by

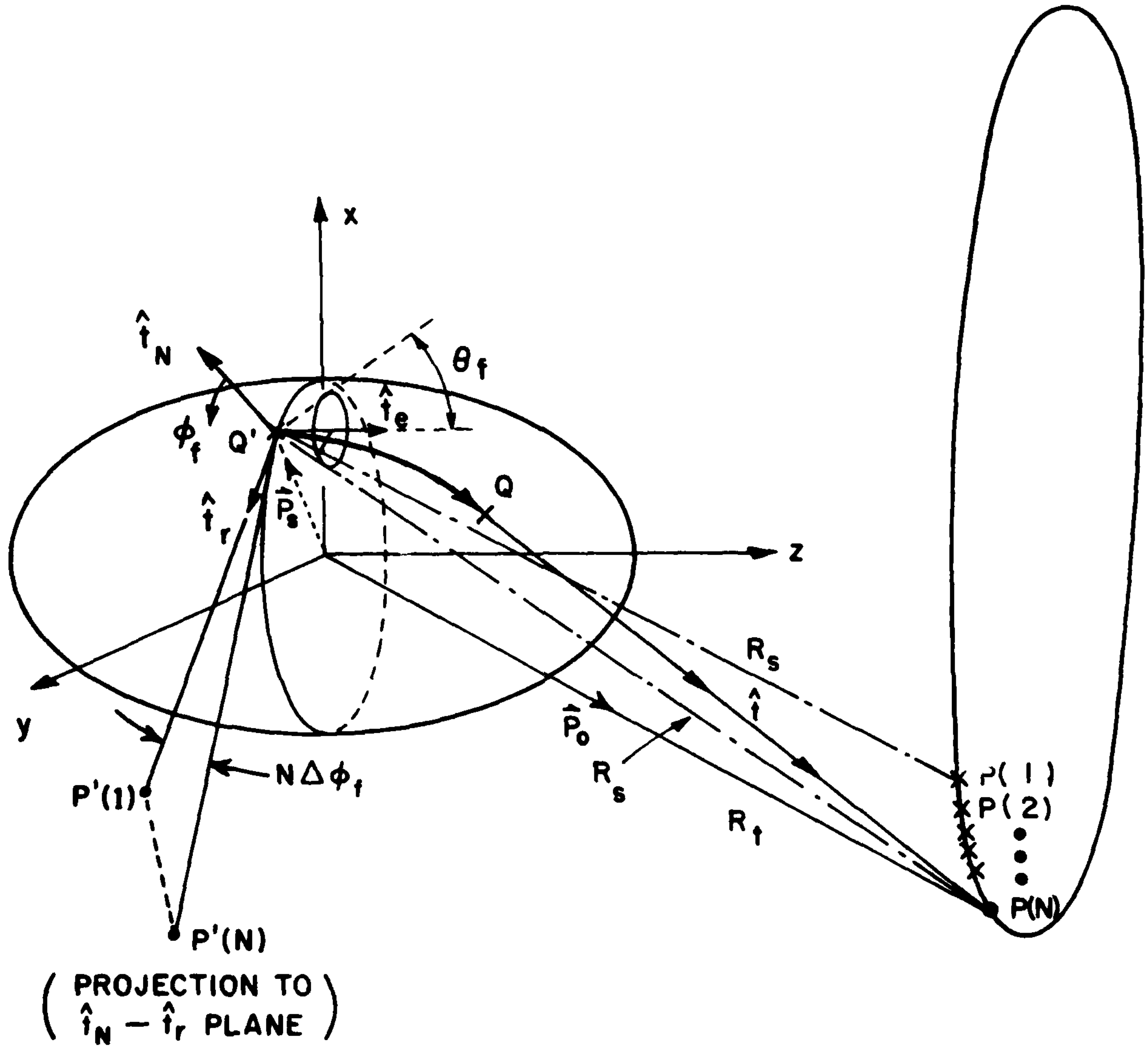

Figure 3. Illustration of the diffraction point finding for a given receiver location.

$$\theta_f = \tan^{-1}\left[\frac{\sqrt{|\hat{t}_N \cdot \vec{P}_{OS}|^2 + |\hat{t}_r \cdot \vec{P}_{OS}|^2}}{\hat{t}_e \cdot \vec{P}_{OS}}\right]$$

with $\vec{P}_{OS} = \vec{P}_O - \vec{P}_S$

and $\phi_f(N)$ is given by

$$\phi_f(N) = \tan^{-1}\left[\frac{\hat{t}_r \cdot \vec{P}_{OS}}{\hat{t}_N \cdot \vec{P}_{OS}}\right] \quad .$$

Note in the figure that P(1) denotes the position vector of the assumed observation point tangential to the source, i.e., $(\theta_f, \phi_f = \frac{\pi}{2})$ with respect to (t_N, t_r, t_e) and P(N) denotes the position vector of the actual observation point tangential to the diffraction point Q, i.e., $(\theta_f, \phi_f + N_{\Delta\phi})$ with respect to $(\hat{t}_N, \hat{t}_r, \hat{t}_e)$ or (θ_t, ϕ_t) with respect to $(\hat{x}, \hat{y}, \hat{z})$. It is observed that there exists a one-to-one correspondence between the points (from P(1) to P(N)) on the rim of the cone and the points on the ellipsoid surface.

After the initial diffraction point is identified by (V_e, V_r); γ, and therefore, the geodesic path is determined by the following equation:

$$\tan \gamma = \frac{S_e}{S_r}$$

since γ is a constant along a given geodesic path on the perturbed elliptic cylinder. Such a numerical approach is illustrated in Figure 4. One need not trace out the complete geodesic path from the source location to the diffraction point for each new radiation direction. As shown in Figure 4, the diffraction point ($V_e+\Delta V_e$, $V_r+\Delta V_r$) for the next receiver location is determined from (V_e, V_r), using Equation (7), if ($\Delta R_t, \Delta\theta_t, \Delta\phi_t$) is small which is the case when a complete radiation pattern is computed.

After the geodesic path is determined, various other parameters associated with actual field calculations must be found. The Fock parameter ξ was obtained in Reference [1] as follows:

$$\xi = \frac{1}{\cos\gamma} \int_{V_{r_s}}^{V_r} \frac{1}{\rho_g} \left(\frac{k\rho_g}{2}\right)^{1/3} \cdot$$

$$\cdot \sqrt{a^2\cos^2V_{es}\sin^2V_r' + b^2\cos^2V_{es}\cos^2V_r'} \quad dV_r'$$

or

$$\xi = \frac{1}{\sin\gamma} \int_{o}^{V_e} \frac{1}{\rho_g} \left(\frac{k\rho_g}{2}\right)^{1/3} \cdot$$

$$\cdot \sqrt{(a^2\cos^2V_r+b^2\sin^2V_r)\sin^2V_e'+c^2\cos^2V_e'} \quad dV_e'$$

where $\rho_g = 1/(k_1\cos^2\gamma + k_2\sin^2\gamma)$ and k_1 and k_2 are two principal curvatures.

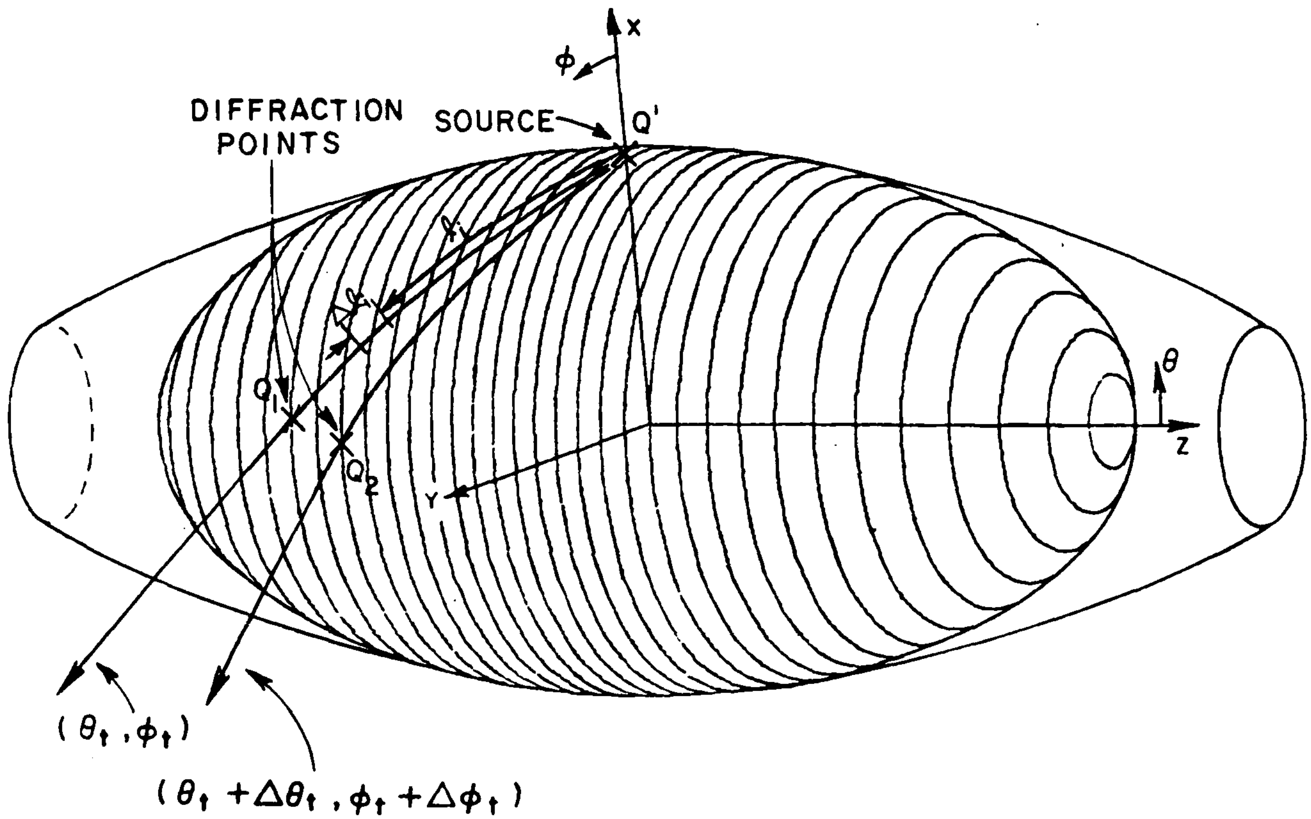

Figure 4. Elliptic cylinder perturbation.

Next, the ray divergence factor $\sqrt{\frac{d\psi_0(Q')}{d\psi(Q)}}$ is defined as the change in the separation of adjacent surface rays as shown in Figure 5. Since the ellipsoid simulating the aircraft fuselage will be long and slender, it is assumed that the ray divergence factor is unity in the analysis.

This completes the elliptic cylinder perturbation solution for the antenna mounted on the mid-section of an ellipsoid.

III. RESULTS

The solutions presented in the previous chapter are employed to compute the near field radiation patterns for short monopoles or slots mounted on the mid-section (θ_s=90°) of an ellipsoid.

To examine different conical pattern cuts, a cartesian coordinate system (x',y',z') originally defining the ellipsoid geometry is now rotated into a new system (x,y,z) as shown in Figure 6. Note that the new cartesian coordinates are found by first rotating about the z'-axis a angle ϕ_c and then about the y-axis a angle θ_c. The pattern is, then, taken in the (x,y,z) coordinate system with θ_p fixed and ϕ_p varied.

To show the validity of the elliptic cylinder perturbation solution, some typical sources, i.e., short monopole, axial slot and circumferential slot, and various source locations are chosen and examined.

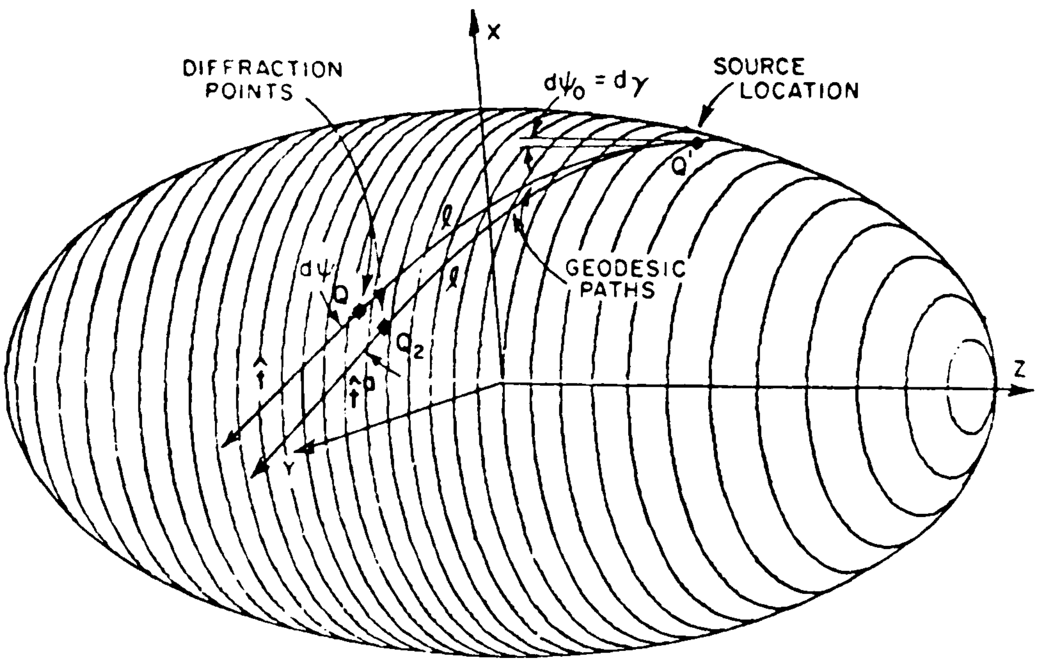

Figure 5. Illustration of the divergence factor ($\sqrt{d\psi_0/d\psi}$) terms.

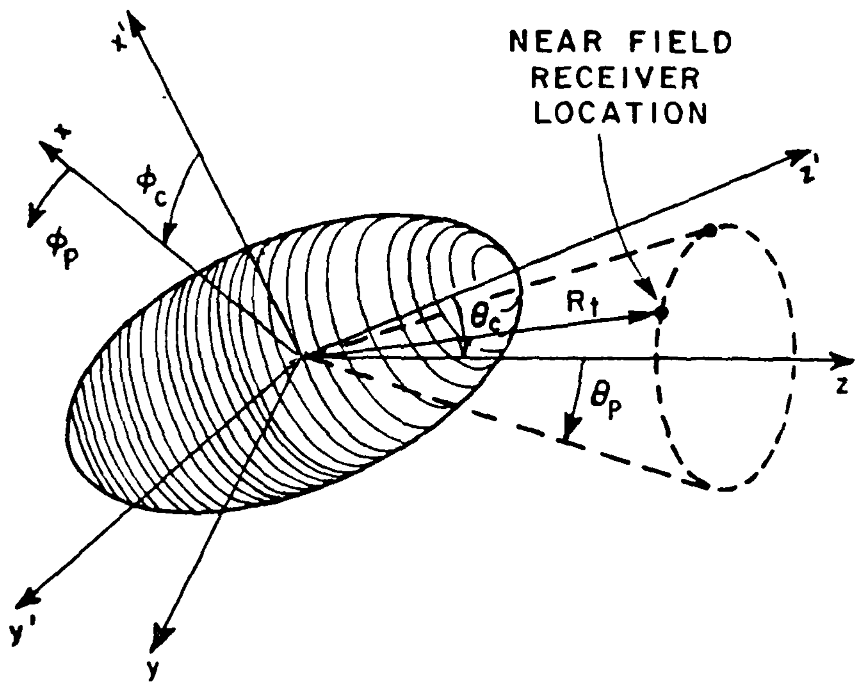

Figure 6. Definition of pattern axis.

For each case the following typical radiation patterns are obtained:

a) $\theta_c = 0°$, $\phi_c = 90°$, $\theta_p = 90°$ (roll plane pattern)

b) $\theta_c = 30°$, $\phi_c = 90°$, $\theta_p = 90°$

c) $\theta_c = 60°$, $\phi_c = 90°$, $\theta_p = 90°$

d) $\theta_c = 90°$, $\phi_c = 90°$, $\theta_p = 90°$ (elevation plane pattern)

e) $\theta_c = 90°$, $\phi_c = 90°$, $\theta_p = 90°$ (azimuth plane pattern).

The radiation patterns obtained by the ellipsoid program, which uses an ellipsoid to simulate the aircraft fuselage, are compared to those obtained using the spheriod solution [4] in each case.

It is noted that the geodesic tracing method of the ellipsoid program for the side mounted antennas (Figures 8, 10, 12, 14, 16, 18) is different from that of the spheroid program because the ellipsoid is not a surface of revolution.

The exact agreement between the results of the ellipsoid program and the spheroid program as shown in Figures 7-12 gives one confidence about the validity of the elliptic cylinder technique.

Next, the ellipsoid program is employed to calculate the radiation patterns due to antennas mounted on an ellipsoid surface. The typical ellipsoid geometry ($2\lambda \times 4\lambda \times 10\lambda$) is chosen and examined for various sources and source locations as shown in Figures 13-18.

The cone boundary shown in Figure 19 is used in determining whether one or two rays are used in the solution. Note that β_{12} is defined automatically by determining the caustic angle in the elevation pattern

(β_c) and adding a few additional degrees to that value, i.e., $\beta_{12} = \beta_c + \Delta\beta$ where $2° < \Delta\beta < 10°$. One would expect to observe slight discontinuities somewhere, because various numbers of rays are included in different regions.

IV. CONCLUSIONS

The object of this study has been to develop an efficient numerical solution for the high frequency radiation patterns of an antenna mounted on the mid-section (Z=0 in Figure 1) of an ellipsoid. The UTD is used in this study to calculate the radiation patterns, and the elliptic cylinder perturbation method is applied to simulate the geodesic paths on the ellipsoid, which in turn can be used to model an aircraft or missile fuselage. For a given radiation direction in the shadow region, the geodesic path and the final diffraction point on the ellipsoid can, then, be found via an efficient numerical approach.

The exact agreement of the radiation patterns from two different programs confirms that this elliptic cylinder perturbation solution is efficient in predicting the high frequency radiation patterns for antennas mounted on the mid-section of an ellipsoid.

This numerical solution will be employed, along with flat plates to construct a general solution for calculating radiation patterns due to airborne antennas.

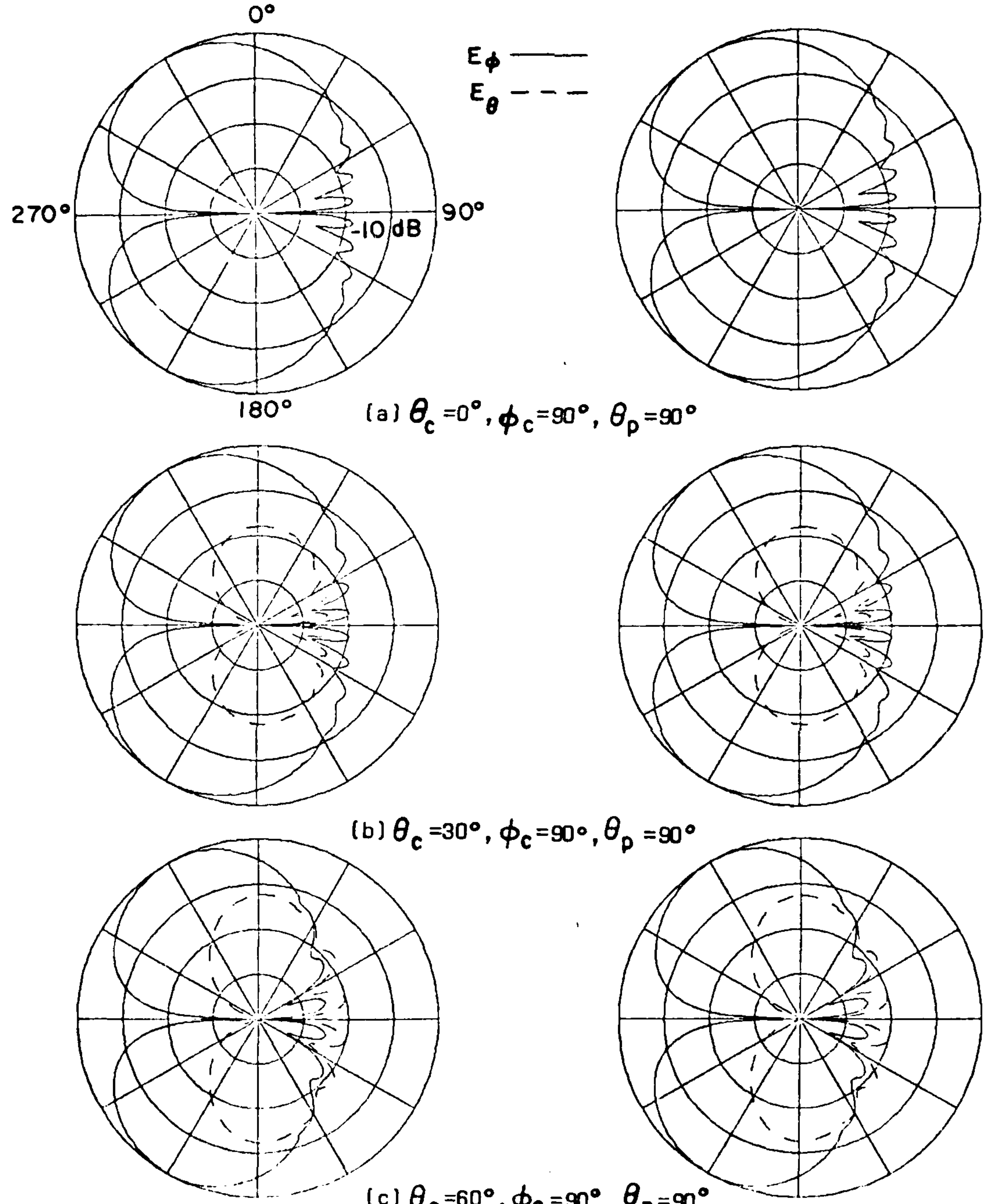

(a) $\theta_c = 0°$, $\phi_c = 90°$, $\theta_p = 90°$

(b) $\theta_c = 30°$, $\phi_c = 90°$, $\theta_p = 90°$

(c) $\theta_c = 60°$, $\phi_c = 90°$, $\theta_p = 90°$

Ellipsoid Program

Spheroid Program

Figure 7. Comparison of radiation patterns for a short monopole mounted at $\phi_s = 0°$, $\theta_s = 90°$ on a $2\lambda \times 10\lambda$ spheriod.

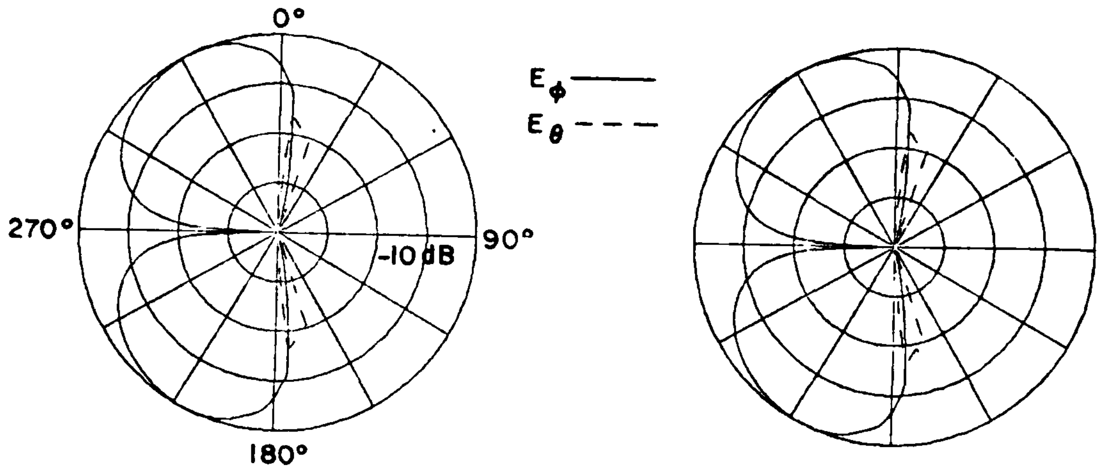

(d) $\theta_c = 90°$, $\phi_c = 90°$, $\theta_p = 90°$

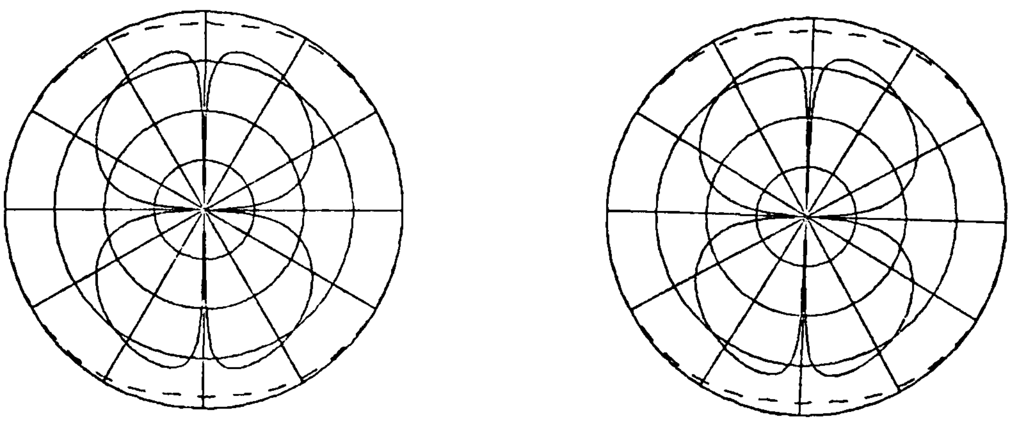

(e) $\theta_c = 90°$, $\phi_c = 0°$, $\theta_p = 90°$

Ellipsoid Program

Spheroid Program

Figure 7. (continued)

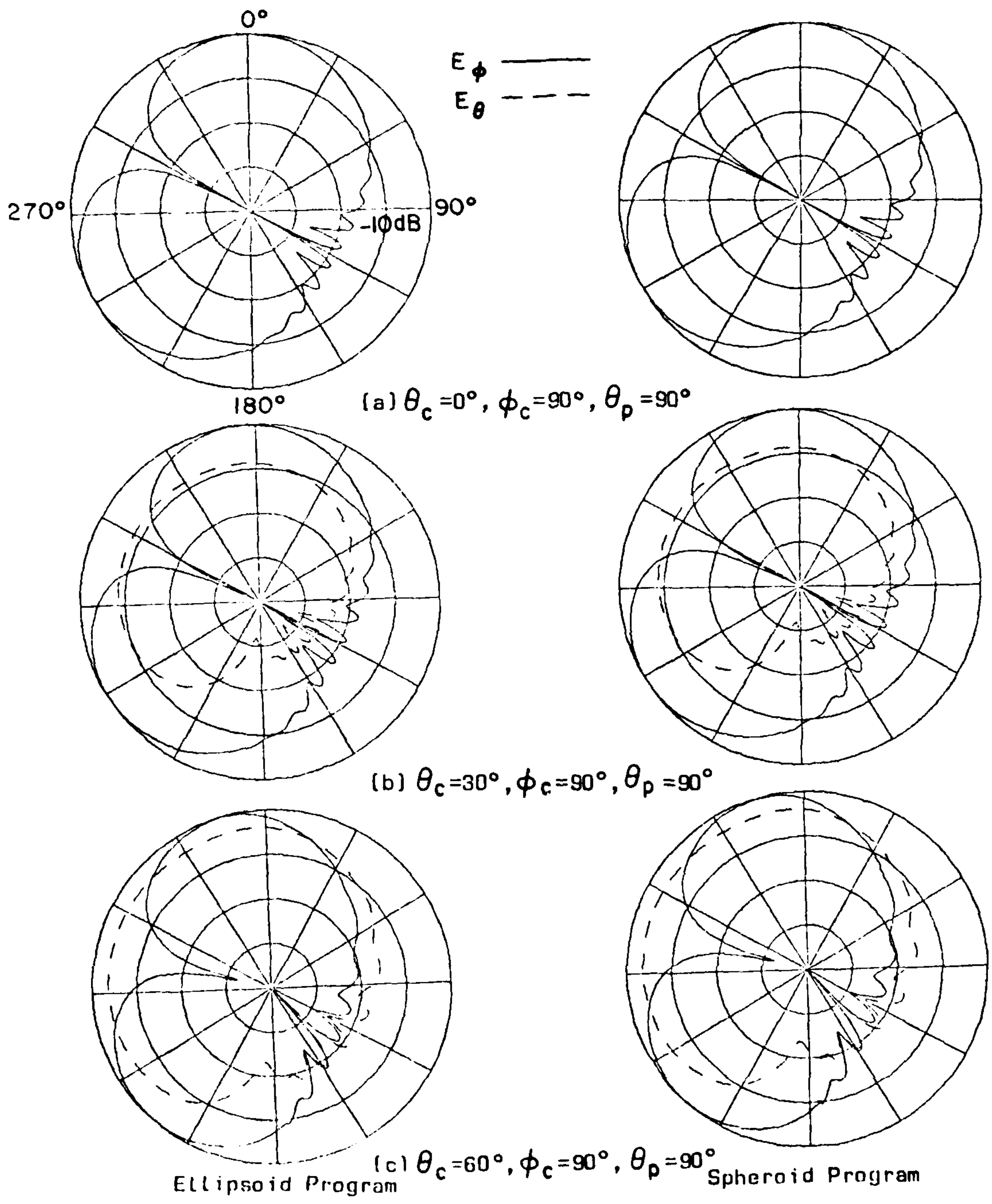

Figure 8. Comparison of radiation patterns for a short monopole mounted at $\phi_s = 30°$, $\theta_s = 90°$ on a $2\lambda \times 10\lambda$ spheriod.

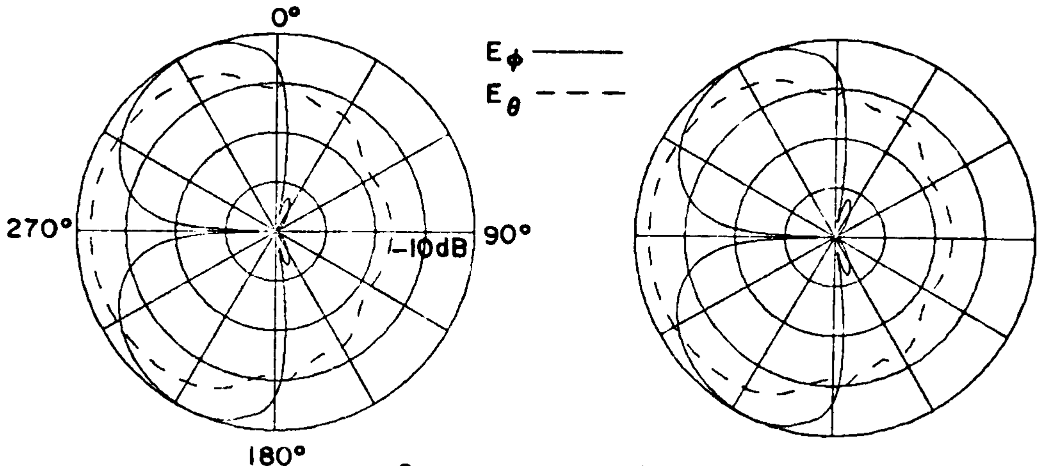

(d) $\theta_c = 90°$, $\phi_c = 90°$, $\theta_p = 90°$

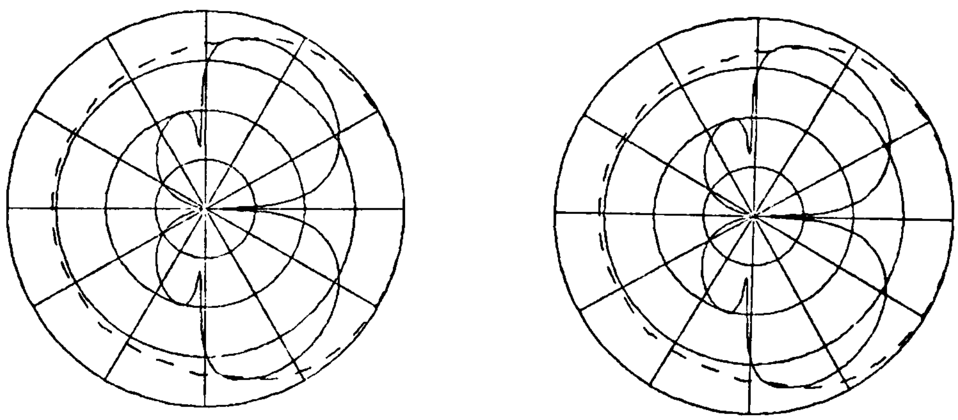

(e) $\theta_c = 90°$, $\phi_c = 0°$, $\theta_p = 90°$

Ellipsoid Program

Spheroid Program

Figure 8. (continued)

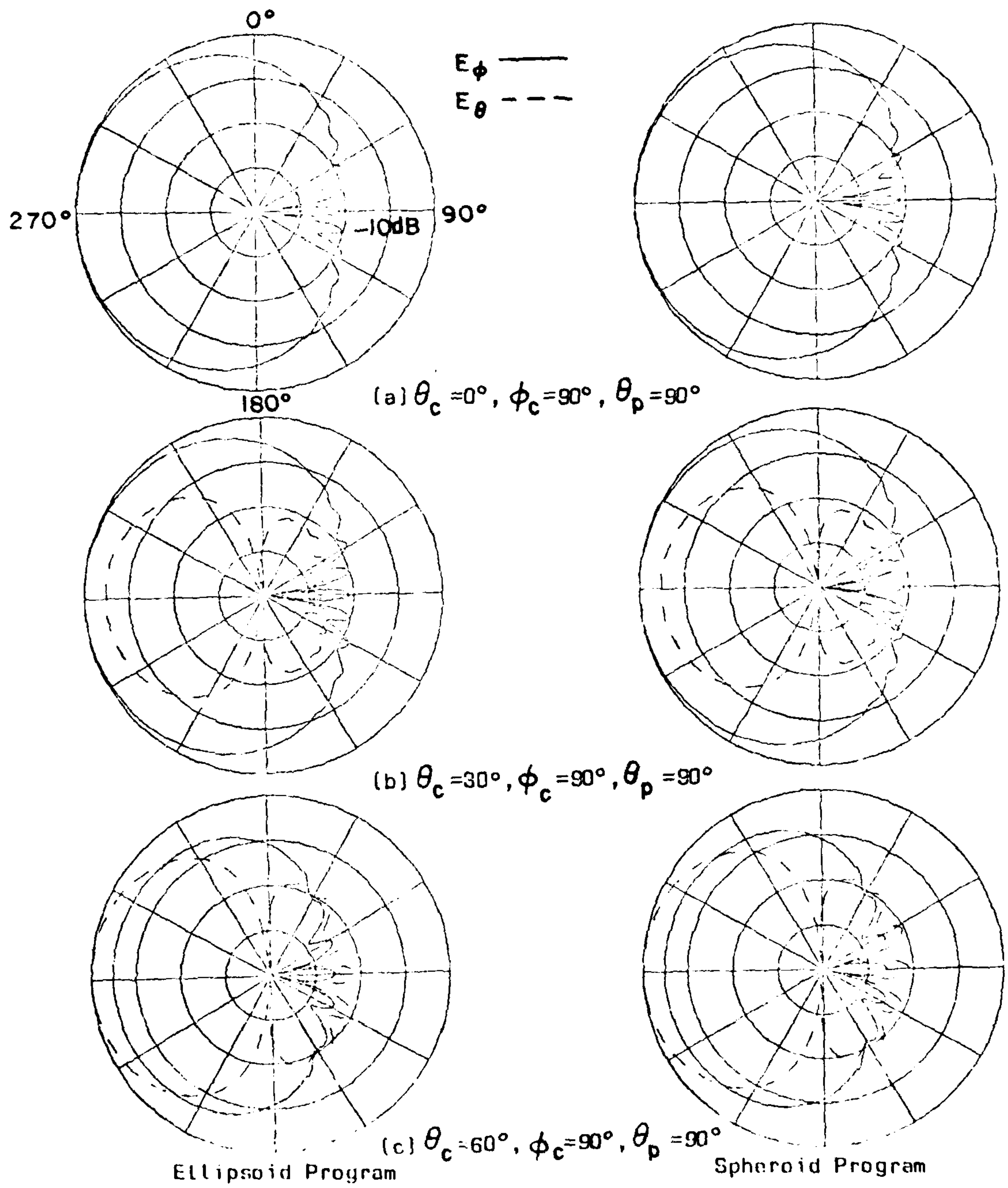

Figure 9. Comparison of radiation patterns for an axial slot mounted at $\phi_s = 0°$, $\theta_s = 90°$ on a $2\lambda \times 10\lambda$ spheriod.

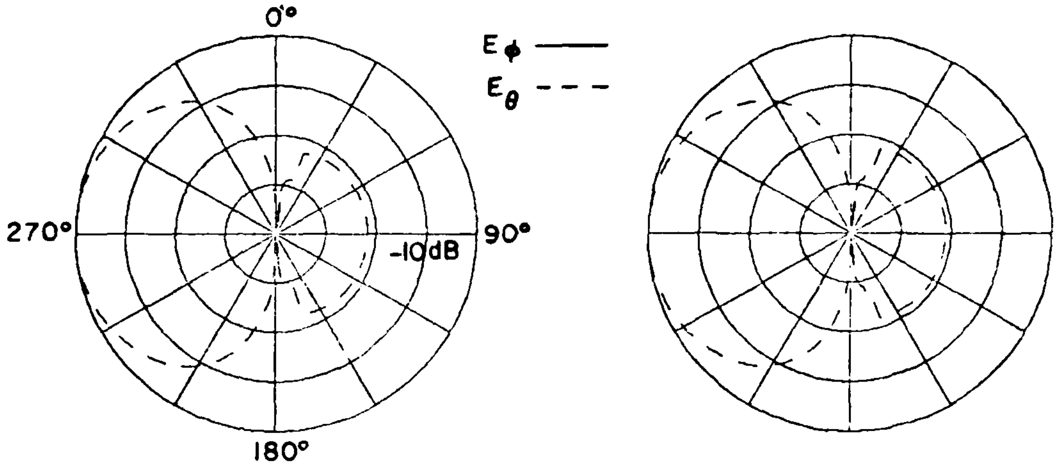

(d) $\theta_c = 90°$, $\phi_c = 90°$, $\theta_p = 90°$

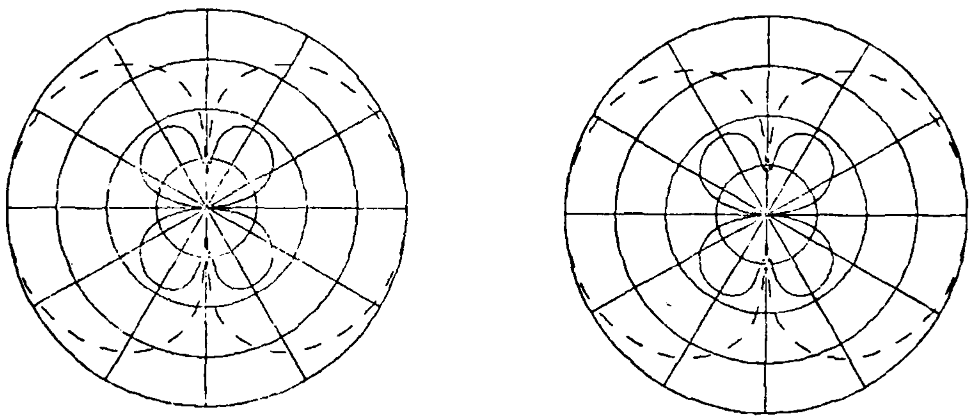

(e) $\theta_c = 90°$, $\phi_c = 0°$, $\theta_p = 90°$

Ellipsoid Program

Spheroid Program

Figure 9. (continued)

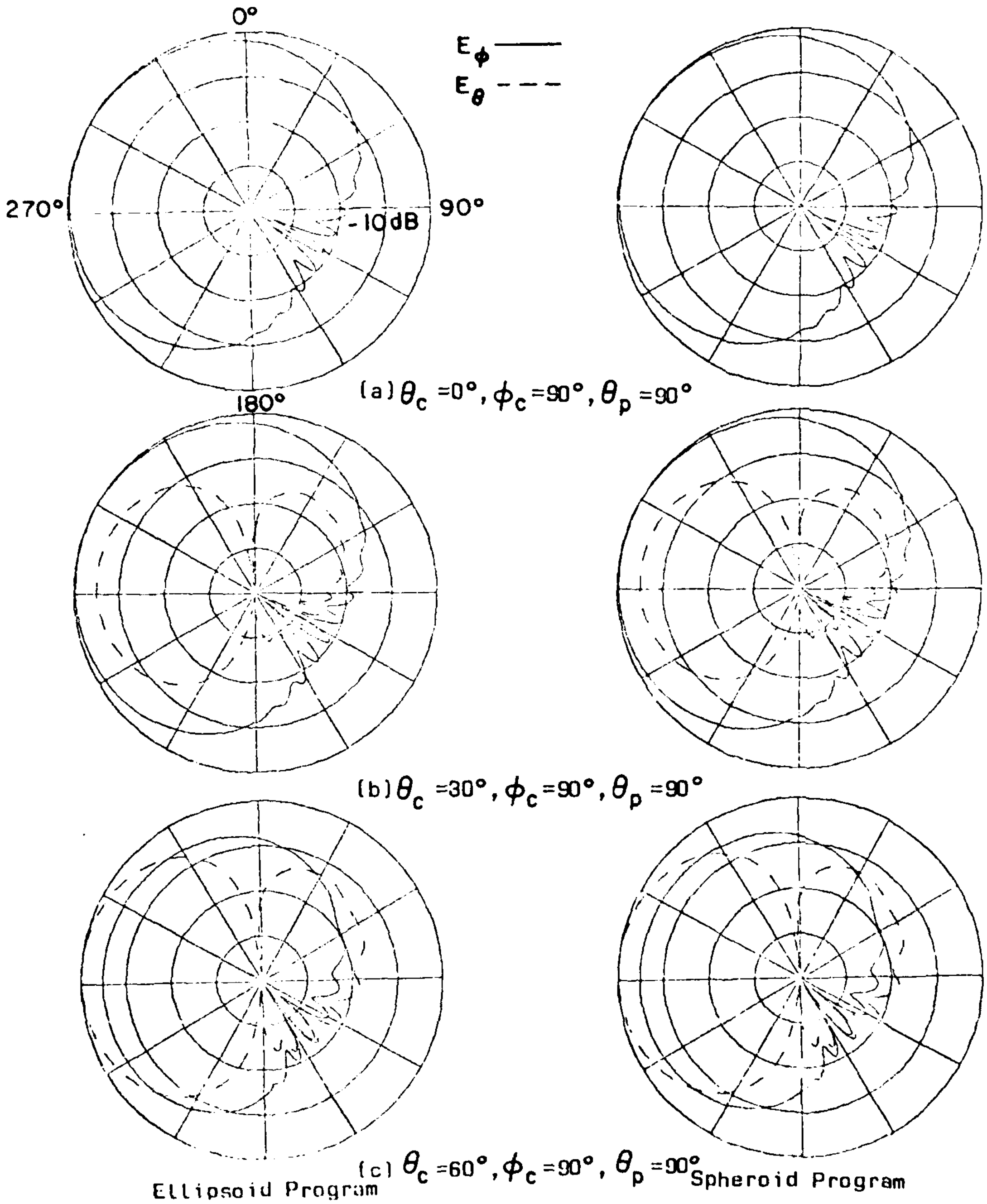

Figure 10. Comparison of radiation patterns for an axial slot mounted at $\phi_s = 30°$, $\theta_s = 90°$ on a $2\lambda \times 10\lambda$ spheriod.

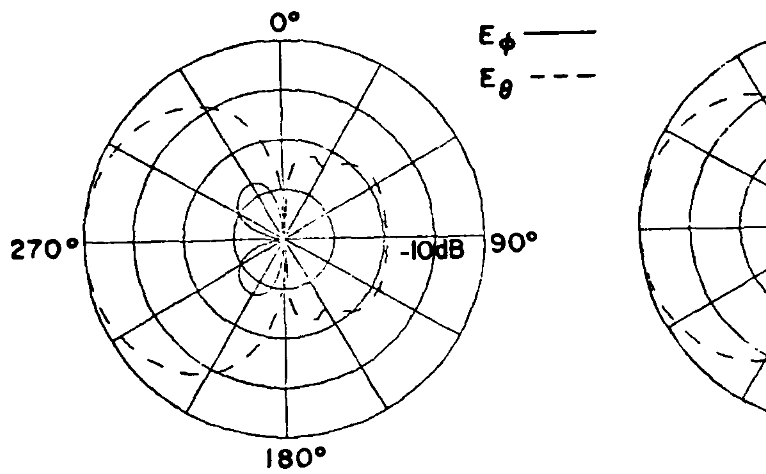

(d) $\theta_c = 90°$, $\phi_c = 90°$, $\theta_p = 90°$

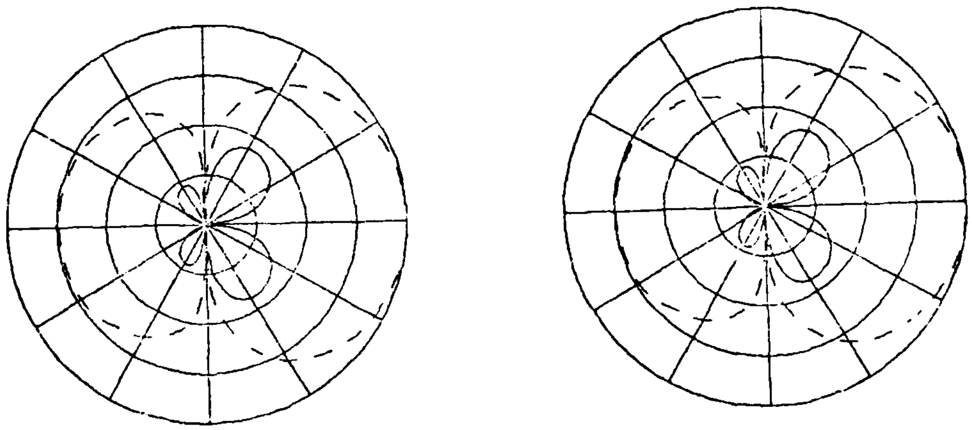

(e) $\theta_c = 90°$, $\phi_c = 0°$, $\theta_p = 90°$

Ellipsoid Program | Spheroid Program

Figure 10. (continued)

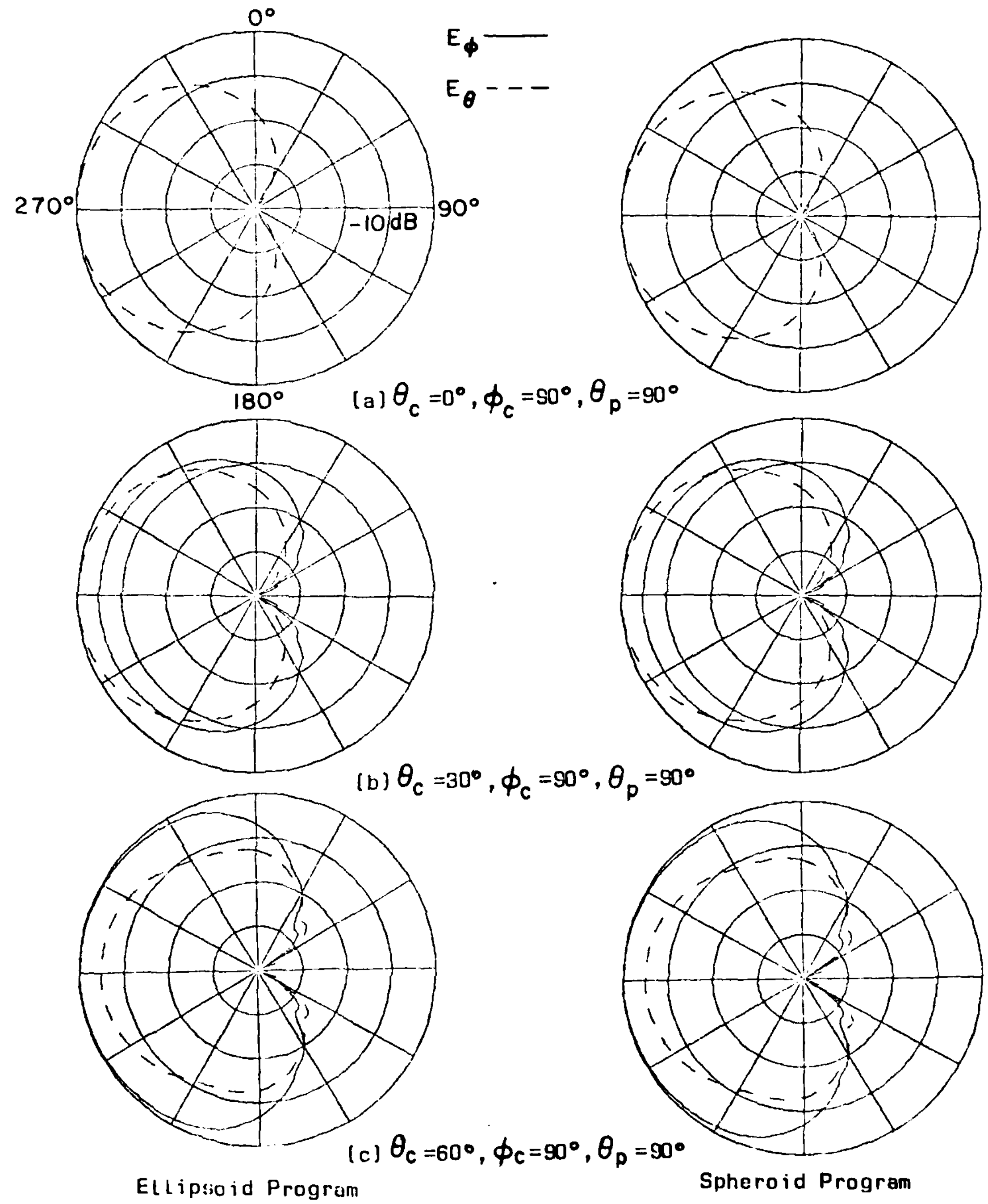

Figure 11. Comparison of radiation patterns for a circumferential slot mounted at ϕ_s = 0°, θ_s = 90° on a 2λ x 10λ spheriod.

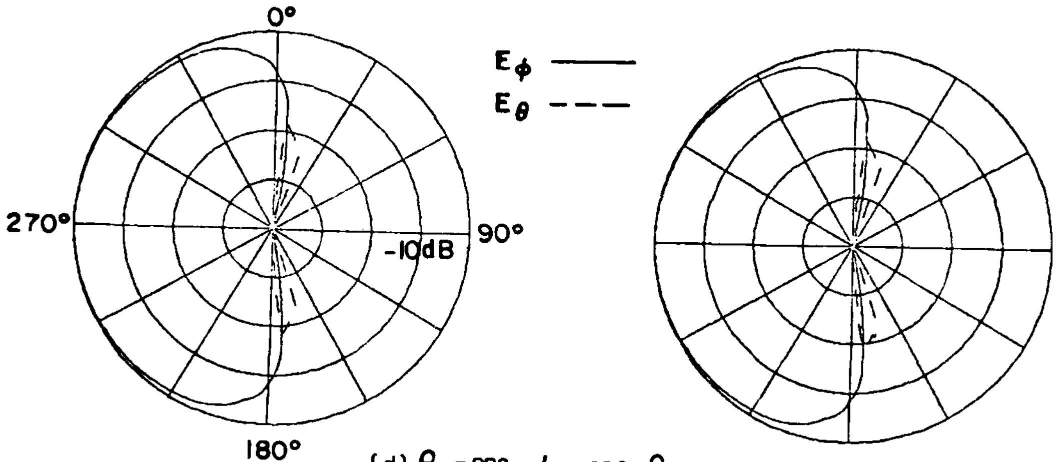

(d) $\theta_c = 90°$, $\phi_c = 90°$, $\theta_p = 90°$

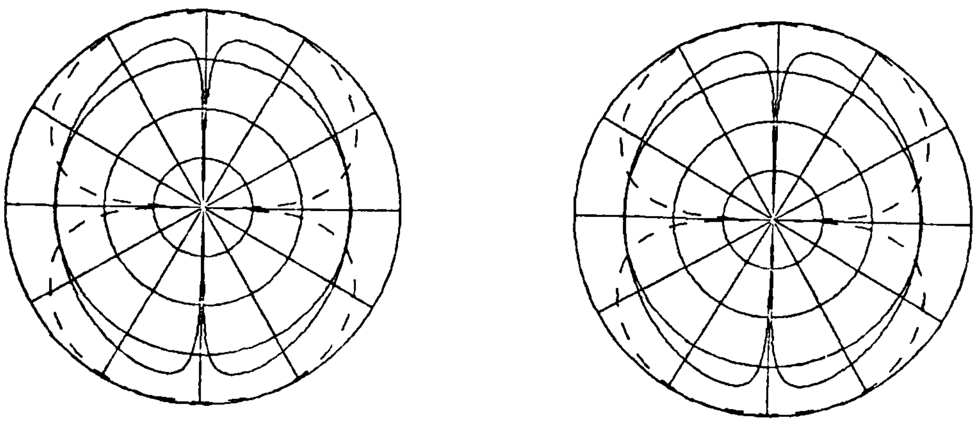

(e) $\theta_c = 90°$, $\phi_c = 0°$, $\theta_p = 90°$

Ellipsoid Program Spheroid Program

Figure 11. (continued)

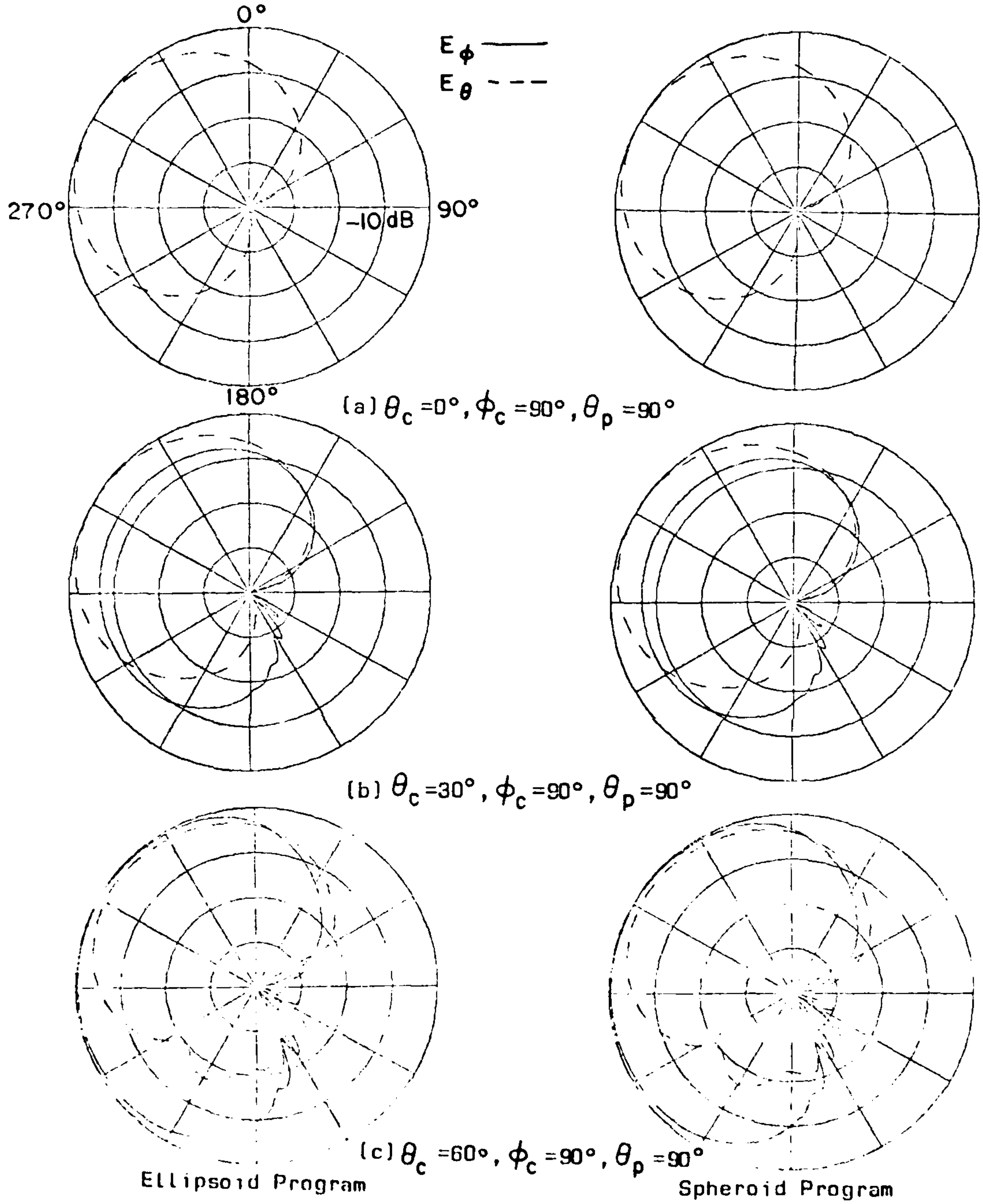

Figure 12. Comparison of radiation patterns for a circumferential slot mounted at $\phi_s = 30°$, $\theta_s = 90°$ on a $2\lambda \times 10\lambda$ spheriod.

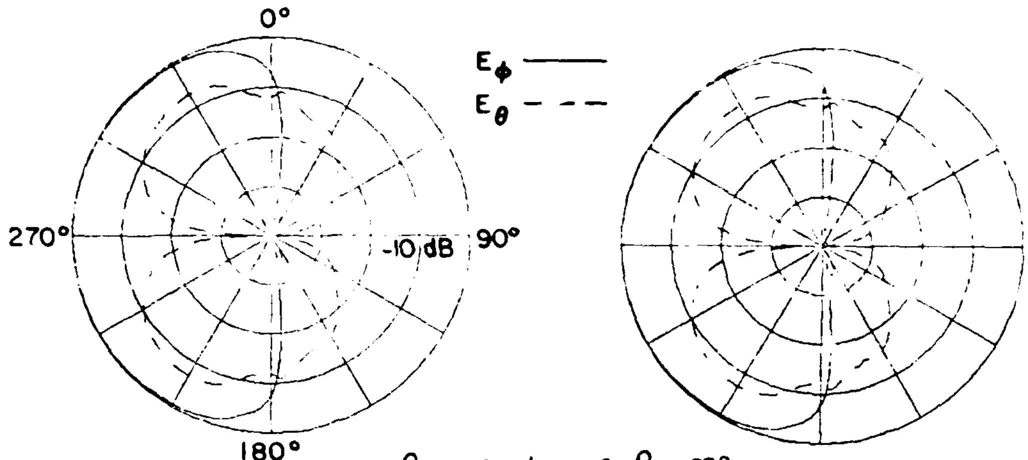

(d) $\theta_c = 90°$, $\phi_c = 90°$, $\theta_p = 90°$

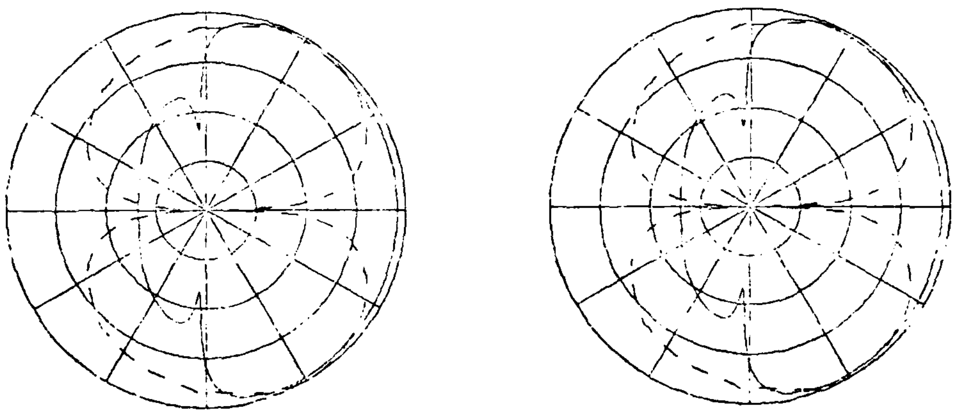

(e) $\theta_c = 90°$, $\phi_c = 0°$, $\theta_p = 90°$

Ellipsoid Program　　　　Spheroid Program

Figure 12. (continued)

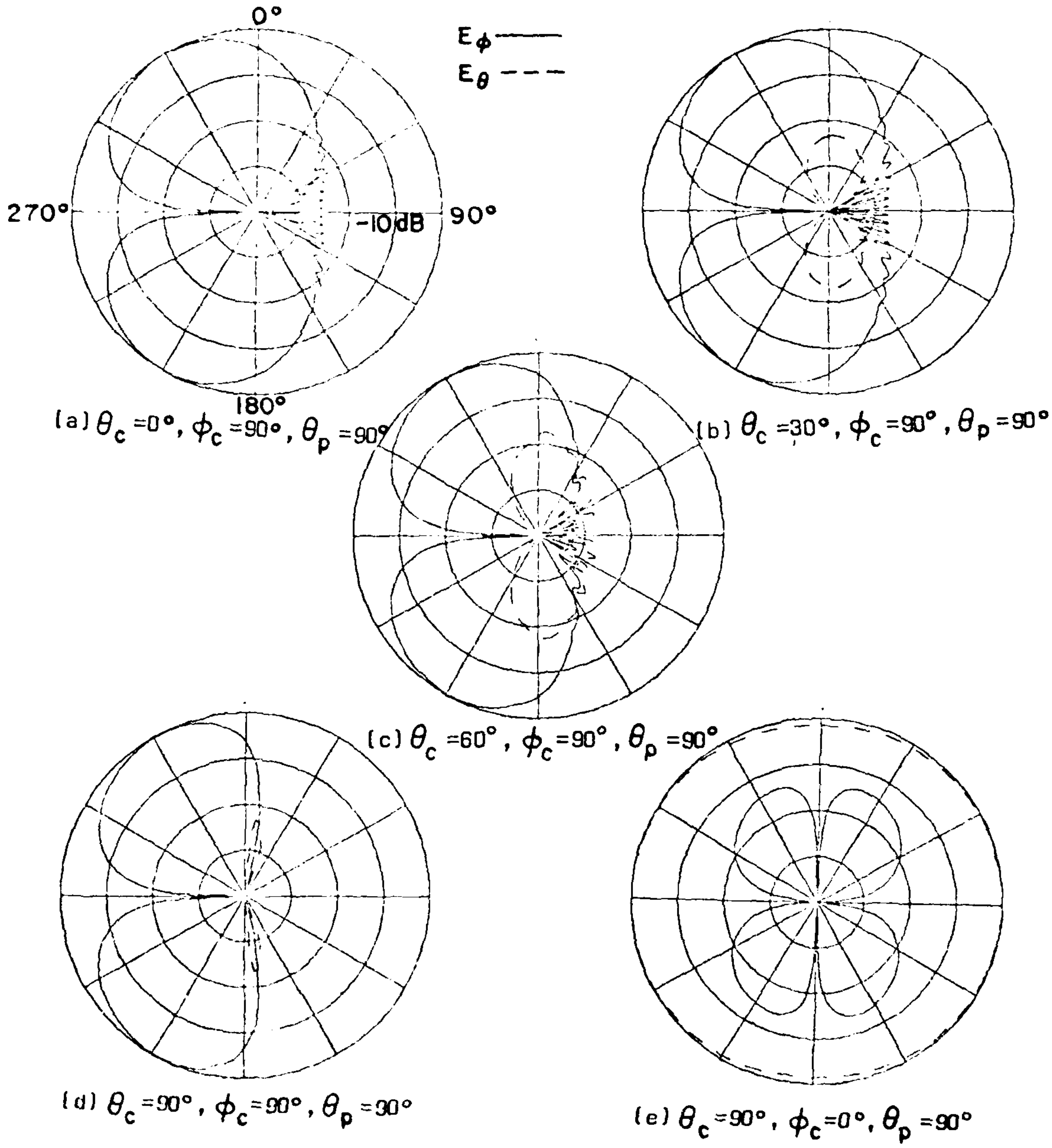

(a) $\theta_c = 0°$, $\phi_c = 90°$, $\theta_p = 90°$

(b) $\theta_c = 30°$, $\phi_c = 90°$, $\theta_p = 90°$

(c) $\theta_c = 60°$, $\phi_c = 90°$, $\theta_p = 90°$

(d) $\theta_c = 90°$, $\phi_c = 90°$, $\theta_p = 90°$

(e) $\theta_c = 90°$, $\phi_c = 0°$, $\theta_p = 90°$

Figure 13. Radiation patterns for a short monopole mounted at $\phi_s = 0°$, $\theta_s = 90°$ on a $2\lambda \times 4\lambda \times 10\lambda$ ellipsoid.

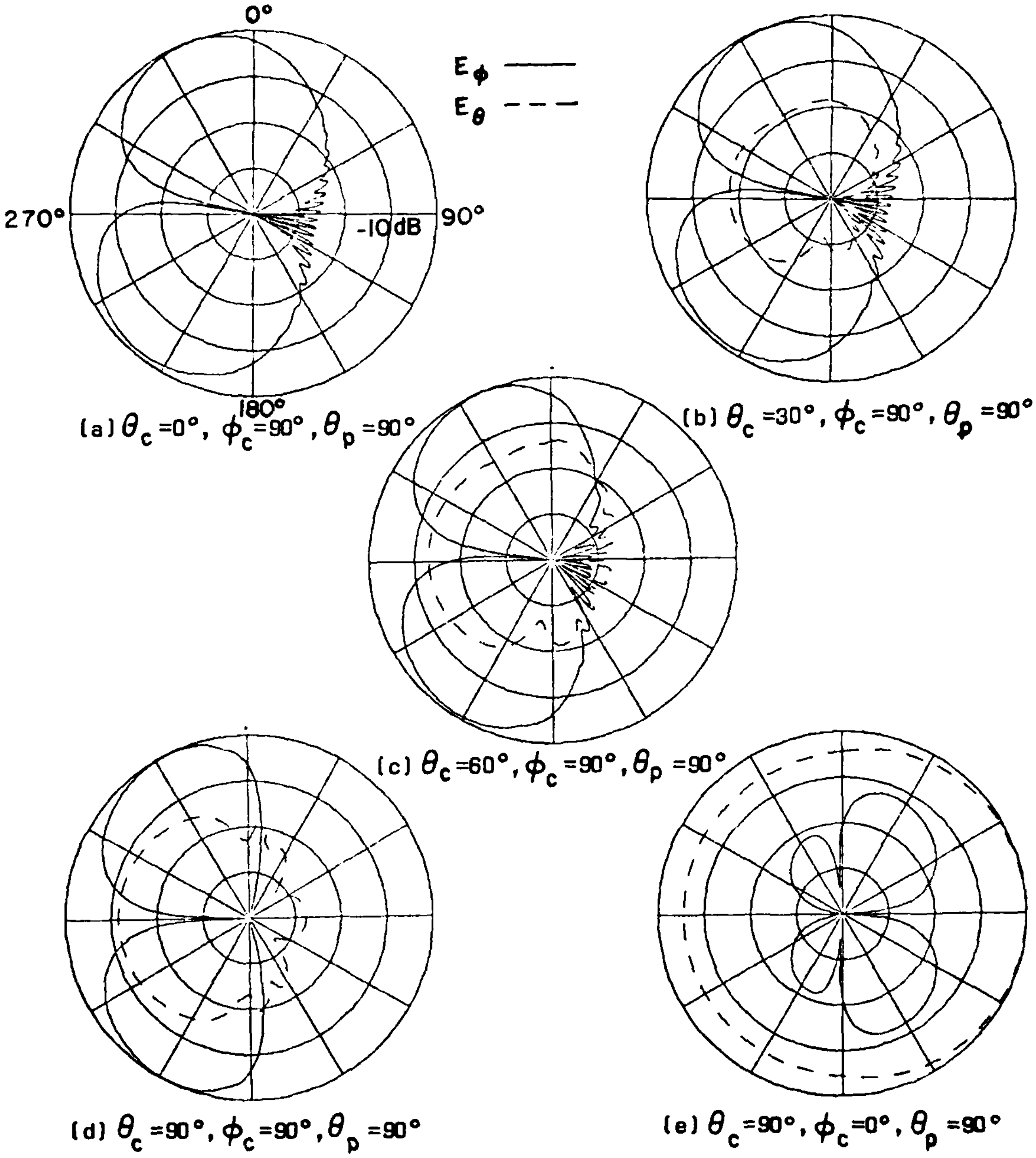

Figure 14. Radiation patterns for a short monopole mounted at $\phi_s = 30°$, $\theta_s = 90°$ on a $2\lambda \times 4\lambda \times 10\lambda$ ellipsoid.

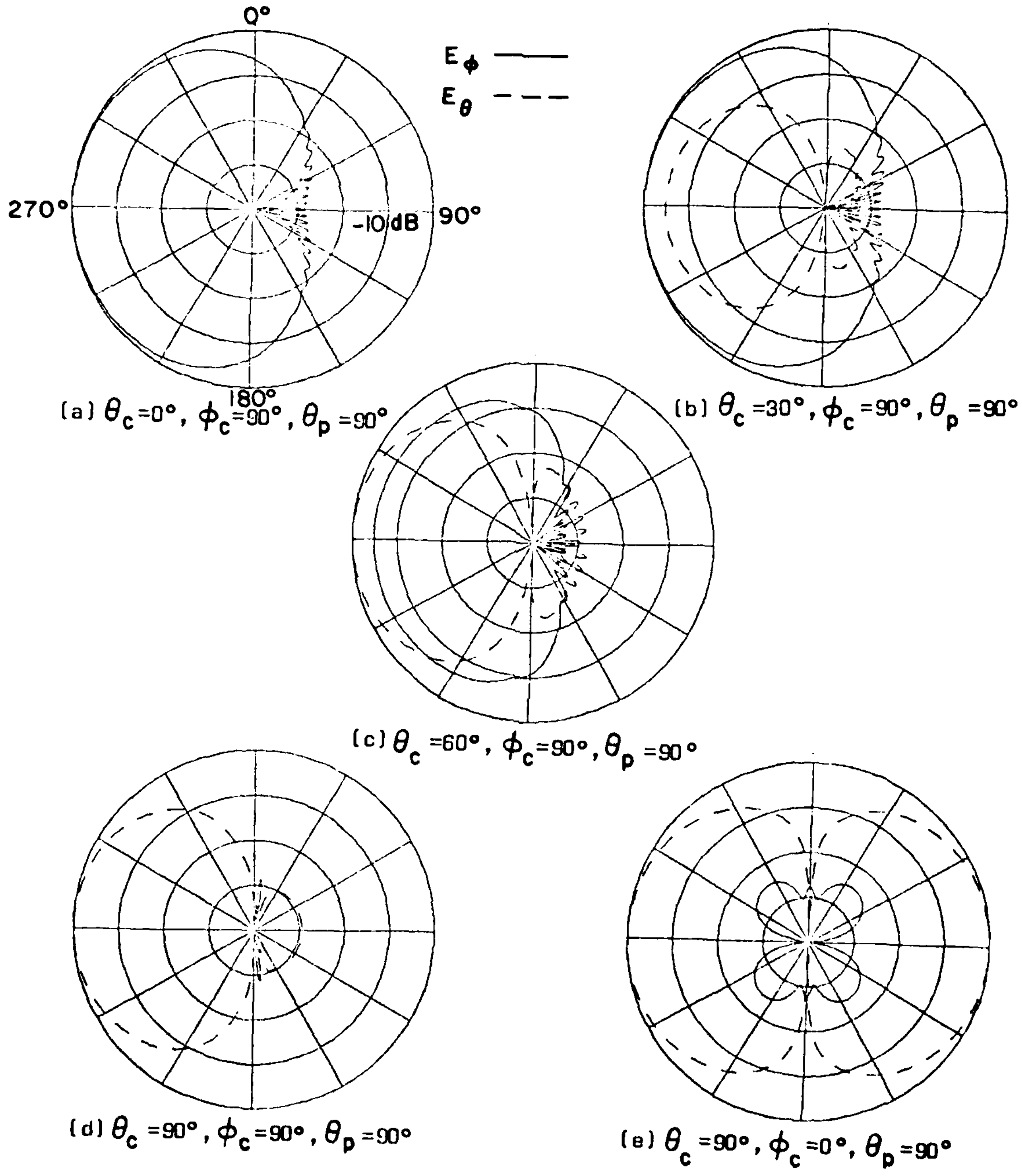

Figure 15. Radiation patterns for an axial slot mounted at $\phi_s = 0°$, $\theta_s = 90°$ on a $2\lambda \times 4\lambda \times 10\lambda$ ellipsoid.

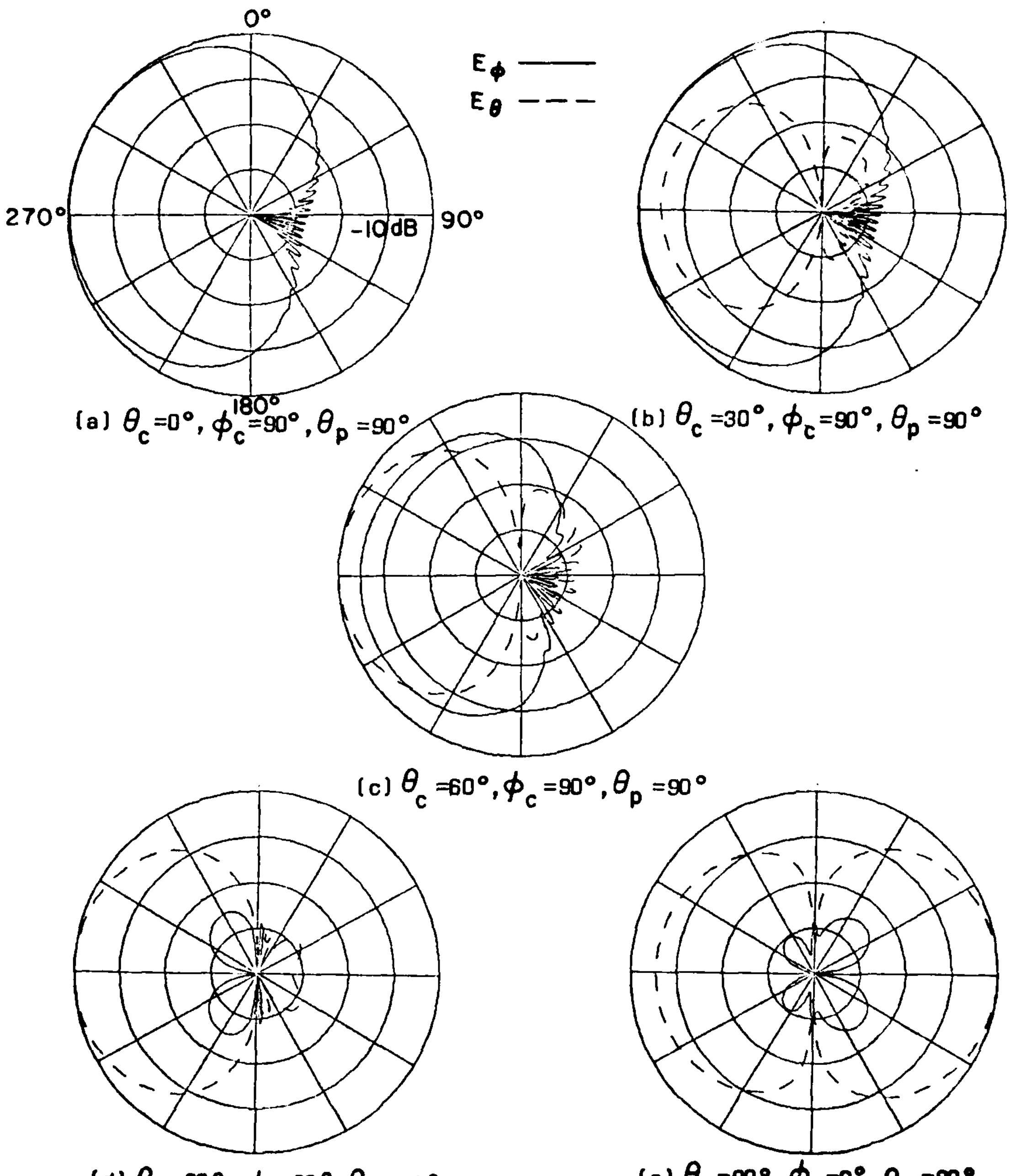

(a) $\theta_c = 0°$, $\phi_c = 90°$, $\theta_p = 90°$

(b) $\theta_c = 30°$, $\phi_c = 90°$, $\theta_p = 90°$

(c) $\theta_c = 60°$, $\phi_c = 90°$, $\theta_p = 90°$

(d) $\theta_c = 90°$, $\phi_c = 90°$, $\theta_p = 90°$

(e) $\theta_c = 90°$, $\phi_c = 0°$, $\theta_p = 90°$

Figure 16. Radiation patterns for an axial slot mounted at $\phi_s = 30°$, $\theta_s = 90°$ on a $2\lambda \times 4\lambda \times 10\lambda$ ellipsoid.

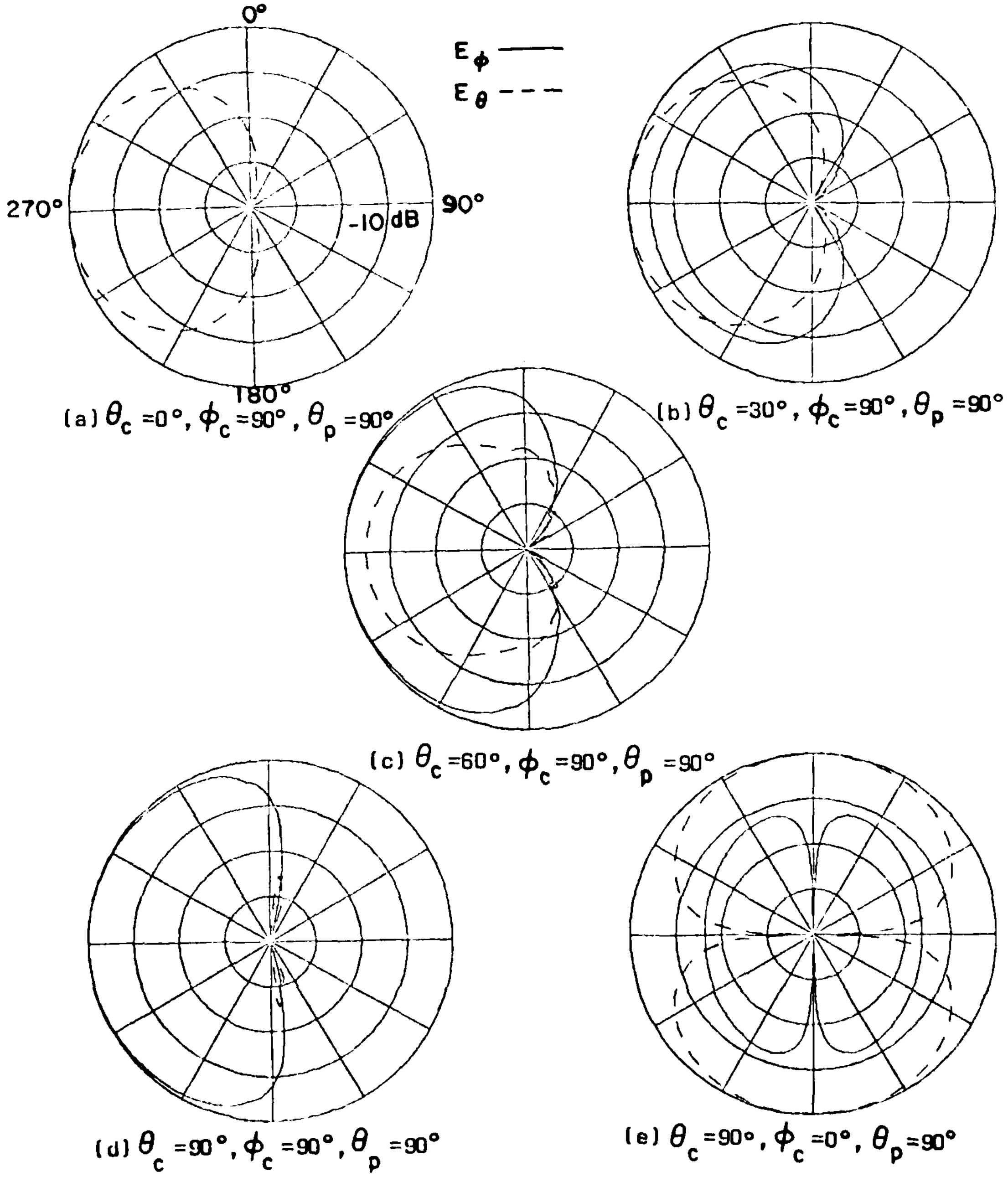

Figure 17. Radiation patterns for a circumferential slot mounted at $\phi_s = 0°$, $\theta_s = 90°$ on a $2\lambda \times 4\lambda \times 10\lambda$ ellipsoid.

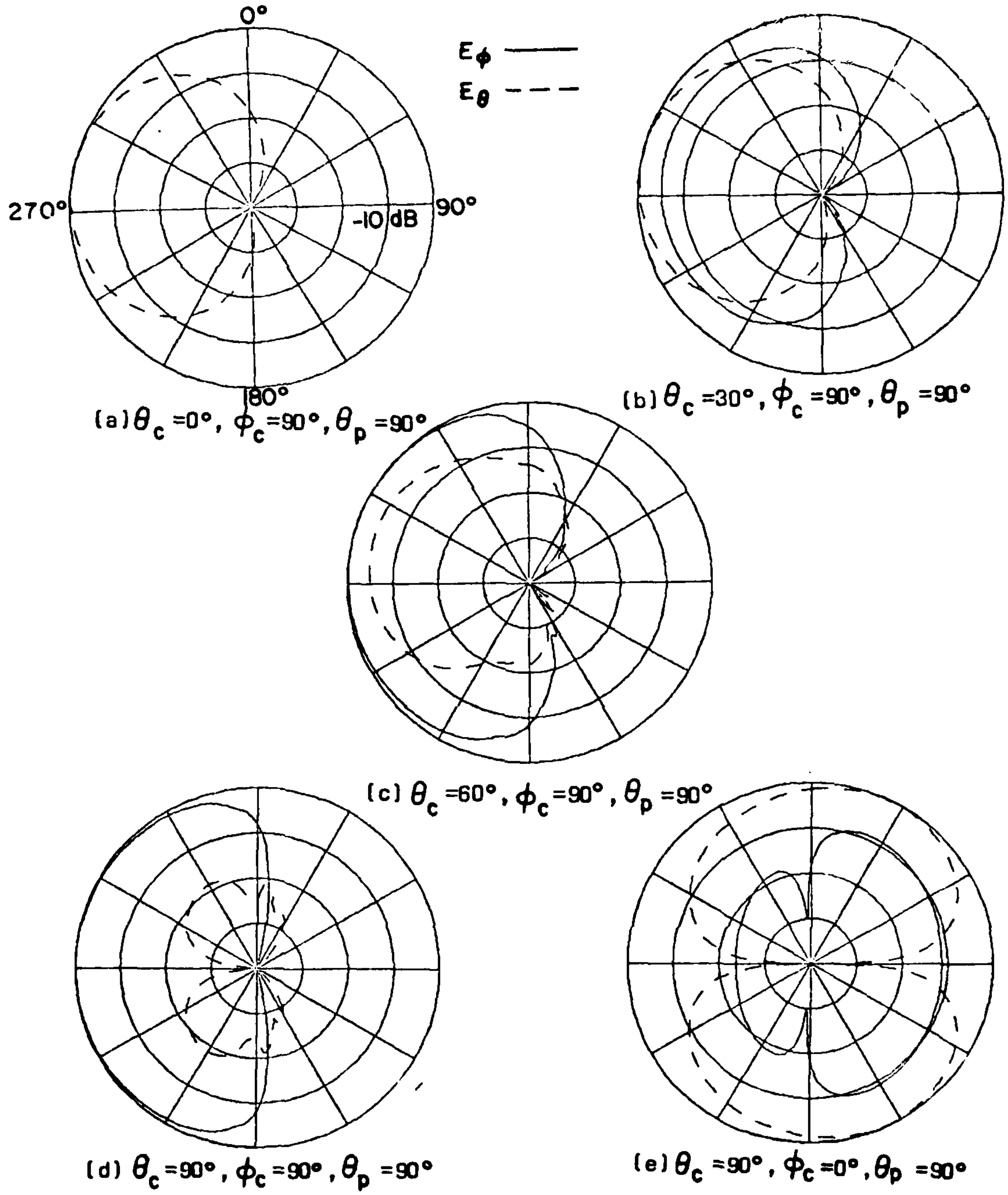

Figure 18. Radiation patterns for a circumferential slot mounted at $\phi_s = 30°$, $\theta_s = 90°$ on a $2\lambda \times 4\lambda \times 10\lambda$ ellipsoid.

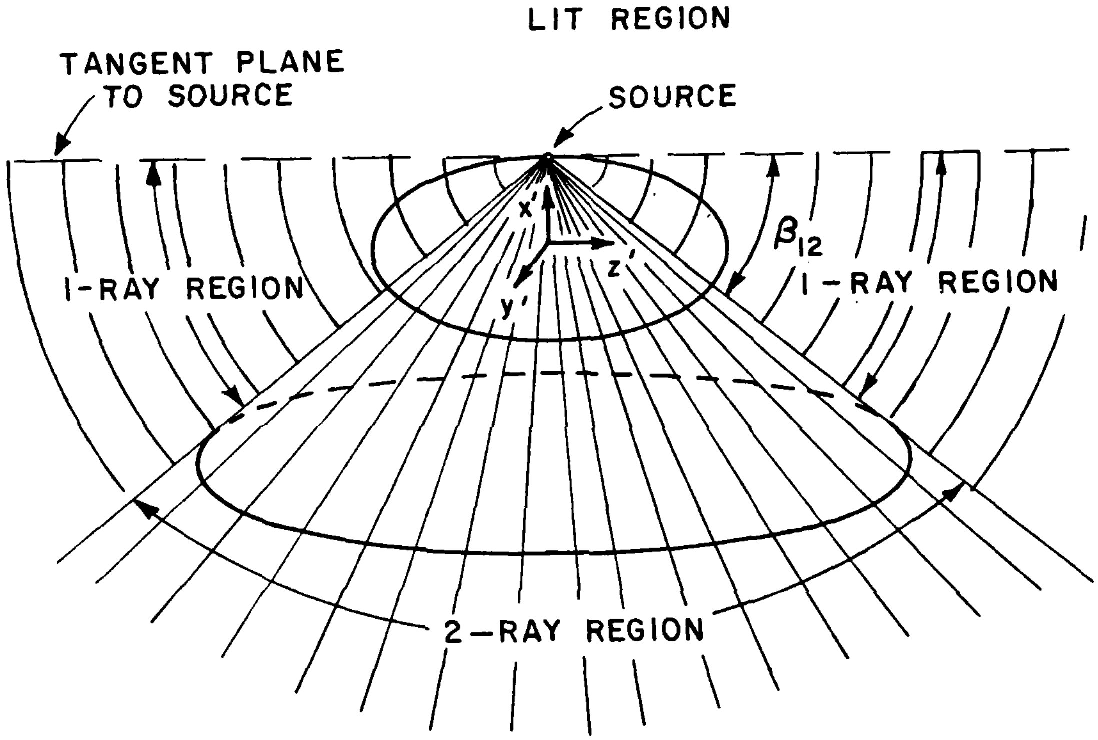

Figure 19. Cone boundary used to define terms to be included in the shadow region.

REFERENCES

[1] J.G. Kim, N. Wang, and C.D. Chuang, "Geodesic Paths of an Ellipsoid-Mounted Antenna", Report 713321-3, The Ohio State University ElectroScience Laboratory, Department of Electrical Engineering; prepared under Contract No. N00019-80-PR-RJ015 for Naval Air Systems Command, March 1982.

[2] J.G. Kim and W.D. Burnside, "Geodesic Paths for Side-Mounted Antenna on an Ellipsoid Model", Report 714215-1, The Ohio State University ElectroScience Laboratory, Department of Electrical Engineering; prepared under Contract No. N00019-81-C-0424 for Naval Air Systems Command, October 1982.

[3] P.H. Pathak, N. Wang, W.D. Burnside, and R.G. Kouyoumjian, "A Uniform GTD Solution for the Radiation from Sources on a Convex Surface", IEEE Trans. and Prop., Vol. AP-29, No. 4, July 1981.

[4] H. Chung, W.D. Burnside, and N. Wang, "The Near Field Radiation Patterns of a Spheroid-mounted Antenna", Report 712527-2, The Ohio State University ElectroScience Laboratory, Department of Electrical Engineering; prepared under Contract No. N00019-81-C-0050 for Naval Air Systems Command, January 1980.

ATE

LMED

8